AD-A091 505 NAVAL RESEARCH LAB WASHINGTON DC F/G 18/3
TWO-DIMENSIONAL FCT MODEL OF LOW-ALTITUDE NUCLEAR EFFECTS.(U)
OCT 80 D L BOOK
UNCLASSIFIED NRL-MR-4362 NL

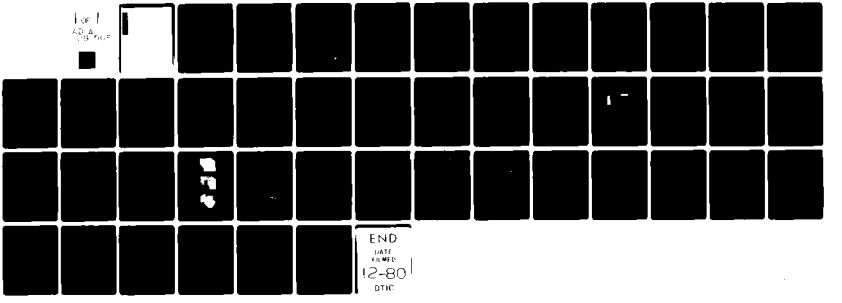

(14) NRL-MR-4362

SECURITY CLASSIFICATION OF THIS PAGE (When Data Entered)

REPORT DOCUMENTATION PAGE

READ INSTRUCTIONS BEFORE COMPLETING FORM

1. REPORT NUMBER: NRL Memorandum Report 4362
2. GOVT ACCESSION NO.: AD-A092
3. RECIPIENT'S CATALOG NUMBER: 505

4. TITLE (and Subtitle): (6) TWO-DIMENSIONAL FCT MODEL OF LOW-ALTITUDE NUCLEAR EFFECTS.
5. TYPE OF REPORT & PERIOD COVERED: Annual Report June 1979 June 1980
6. PERFORMING ORG. REPORT NUMBER:

7. AUTHOR(s): (10) D.L. Book (16) Y99QAXS
8. CONTRACT OR GRANT NUMBER(s): (11) 26 Oct 80

9. PERFORMING ORGANIZATION NAME AND ADDRESS: Naval Research Laboratory, Washington, D.C. 20375 — 61101A
10. PROGRAM ELEMENT, PROJECT, TASK AREA & WORK UNIT NUMBERS: 62-0578-0-0 (12) 46

11. CONTROLLING OFFICE NAME AND ADDRESS: Defense Nuclear Agency, Washington, D.C. 20305 (17) 6602
12. REPORT DATE: October 16, 1980
13. NUMBER OF PAGES: 45

14. MONITORING AGENCY NAME & ADDRESS (if different from Controlling Office): (9) Annual rept. 1 Jun 79-1 Jun 80,
15. SECURITY CLASS. (of this report): UNCLASSIFIED
15a. DECLASSIFICATION/DOWNGRADING SCHEDULE:

16. DISTRIBUTION STATEMENT (of this Report)

Approved for public release; distribution unlimited.

17. DISTRIBUTION STATEMENT (of the abstract entered in Block 20, if different from Report)

18. SUPPLEMENTARY NOTES

This work was supported by the Defense Nuclear Agency under subtask Y99QAXSG601, work unit 22, and work unit title "B11 Flux-Corrected Transport Code."

19. KEY WORDS (Continue on reverse side if necessary and identify by block number)

Shock waves
Mach shocks
Shock reflection
Height of burst
Vulnerability

20. ABSTRACT (Continue on reverse side if necessary and identify by block number)

Low-yield experiments with chemical explosives detonated at low altitude have revealed unusual Mach stem structures. Existing codes employed to simulate these phenomena have been unable to resolve them satisfactorily. During the year beginning 1 June 1979, personnel of the Laboratory for Computational Physics have been working under a contract with the Defense Nuclear Agency to develop software for performing these calculations.

Abstract (continues)

DD FORM 1 JAN 73 1473 EDITION OF 1 NOV 65 IS OBSOLETE
S/N 0102-LF-014-6601

SECURITY CLASSIFICATION OF THIS PAGE (When Data Entered)

252950

20. Abstract (continued)

For this purpose, we have employed the method of Flux-Corrected Transport (FCT), developed at the Naval Research Laboratory by J.P. Boris and D.L. Book.

CONTENTS

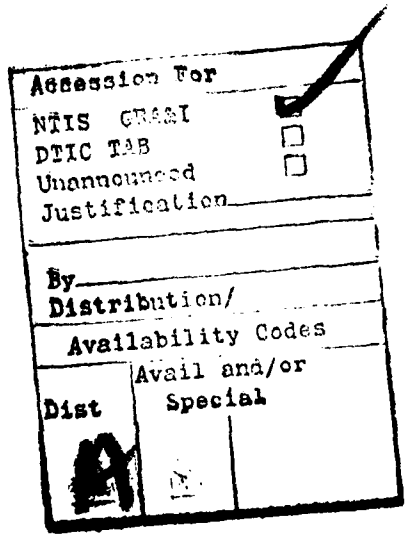

TWO-DIMENSIONAL FCT MODEL OF LOW-ALTITUDE NUCLEAR EFFECTS

I. INTRODUCTION

Low-yield experiments with chemical explosives detonated at low altitude have revealed unusual Mach stem structures. Existing codes employed to simulate these phenomena have been unable to resolve them satisfactorily. During the year beginning 1 June 1979, personnel of the Laboratory for Computational Physics have been working under a contract with the Defense Nuclear Agency to develop software for performing these calculations. For this purpose we have employed the method of Flux-Corrected Transport (FCT), developed at NRL by J. P. Boris and D. L. Book.[1-4]

The thrust of the program during the first year has been toward testing the various alternative forms of FCT which have been developed, with a view to designing an optimum code (or codes) for solving airblast problems. The principal features we have tried to investigate and evaluate are (1) adaptive regridding; (2) multidimensional (i.e., not time-split) flux limiting;[5] (3) the use of ZIP differencing in calculating fluxes;[6] (4) the use of spatially higher-order (6th-order, 8th-order, etc.) difference schemes as a basis for designing the FCT routine. We concluded that (1) and (2) are definitely efficacious; (1) indeed is indispensable for some problems. We found strong indications that (3) is ineffective on the problems studied, while we have thus far not tested (4) and have only indirect evidence in favor of using high-order methods. In this report we will discuss only calculations related to testing (1) and (2).

The plan for FY-80 listed four milestones: (1) Implement adaptive rezone in Cartesian coordinates; (2) Apply code to model test problem (plane shock

Manuscript submitted August 26, 1980

above ramp); (3) Convert code to cylindrical coordinates; (4) Apply code to model test problem (0.5 ton HE at 5 m height).

All of these have been carried out and are described below. In addition, we have implemented a vectorized real-air equation-of-state routine, permitting us to estimate the importance of real gas effects on airblast calculations.

Section II of this report describes the code development work we have performed [items (1) and (3) in the above list]. Section III describes our shock-on-wedge calculations [item (2)]. Section IV describes our work on height-of-burst studies; however, the parameters employed in the test cases differ from those specified above. The text of a paper[7] describing some of the results obtained in this program, presented at the Seventh International Conference on Numerical Methods in Hydrodynamics held during 25-27 June in Stanford, is included as an appendix to the report.

Work is continuing during the remainder of the fiscal year to extend and refine the results reported here.

II. CODE MODIFICATION AND DEVELOPMENT

A. Leapfrog -- Trapezoidal Code

A 2D Cartesian leapfrog-trapezoidal code written under DNA support by Zalesak for ionospheric striation studies was used as the starting point in developing a reflecting shock code. This was done by disabling certain features (magnetic fields, gravitational potential) specific to the original problem, and writing initialization and boundary condition routines appropriate to the shock problem.

In its present form the code solves the ideal fluid equations on a fixed uniform mesh, using an unsplit 2D FCT transport routine. This routine can embody either a leapfrog or a trapezoidal finite-difference scheme. The former is (linearly) reversible and time-centered and has unit linear amplification, but is subject to weak (grid-separation) instability. This is corrected by calling the trapezoidal scheme at intervals (typically every five timesteps) to "merge" the separating solutions.

A perfectly reflecting boundary condition applied at the bottom of the mesh represents the wedge surface; the incident shock front makes an angle θ_w with the vertical, equal to the wedge angle. On the other boundary cells, values of the density ρ, pressure p, and velocity v are assigned their values in the ambient gas ahead or behind the incident shock, depending on where they are located with respect to the known shock position at that time.

Results of the calculations (arrays of the fluid quantities) are dumped on magnetic tape at intervals of ten timesteps. Graphics (contour plots, time histories of sensors at fixed locations, etc.) are obtained by postprocessing the data tape.

B. FAST2D

FAST2D is a two-dimensional timesplit FCT fluid code developed by Boris[8] for reactive flow and hydrodynamic stability calculations. For the present task it was utilized in a configuration very similar to that of the Leapfrog-Trapezoidal code. Initial and boundary conditions were applied in identical fashion.

The FAST2D chemistry routines were omitted, but the dynamic rezone capability was retained in most of the calculations. The latter exploits the improved resolution obtainable by fine-gridding the portion of the mesh containing the most important or most intransigent part of the calculation --in this case, the region in which the Mach stem(s) and triple point(s) are located (Fig. 1). Coarse gridding, which reduces the core and running-time requirements, provides adequate resolution on the less sensitive remainder of the mesh.

The most important feature of the rezone is its ability to track the critical region. This means that the calculation is effectively carried out in the reference frame of the leading Mach stem. In calculations with glancing incident shocks, where the opening angle α is as small as one or two degrees, the triple point must move a long way (several hundred cells on a uniform mesh) before it is far enough above the wedge (5-10 cells) to be resolved satisfactorily. With the dynamic rezone, only $\sim$ 150 cells need to be used in the calculation.

C. Real-Air Equation of State

A routine provided by A. Kuhl (RDA) which calculates the effective ratio of specific heats (adiabatic index) γ in a variety of situations of interest for airblast problems[9] has been converted to run on the NRL TI/ASC. In its original form this routine accepts values of specific internal energy ϵ and density ρ

and returns γ, temperature T and pressure p according to four prescriptions: (1) a table lookup for dry real air, valid from room temperature to $\sim 10^7$K and from millitorr to kilobar pressures; (2) a polynomial fit to these data; (3) an analogous formula for detonation products from the high explosive Atlas Aquanel; and (4) the values appropriate to an ideal gas (constant gamma). The NRL version is vectorized; it accepts arrays of values of ϵ and ρ and returns corresponding arrays of γ, T, and p. The resulting code runs approximately two orders of magnitude faster in mode (1) than the original version, and has been used with both the Leapfrog-Trapezoidal and FAST2D codes to calculate the "real air" cases described below.

III. SHOCK-ON-WEDGE CALCULATIONS

This section briefly describes the results of the principal calculations we have performed on shocks reflecting from wedges. The runs reported here (summarized in Table 1) are discussed in three categories: small wedge angles, large (i.e., $\gtrsim 45^{\circ}$) wedge angles, and runs carried out for the purpose of comparing two codes or models. The types of Mach reflection to be expected can be found from Fig. 2, which divides the parameter space into seven distinct regions.

A. Small Wedge Angles

For small wedge angles (i.e., glancing incident shocks), the opening angle α is $\sim 10^{\circ}$ and resolution of the Mach shock region presents no great difficulty. The Leapfrog-Trapezoidal code was used to perform two calculations of this sort (filled circles in Fig. 2), both with an ideal-gas EoS. The wedge angles were $\theta_w = 26.56^{\circ}$ and $\theta_w = 20^{\circ}$; the Mach numbers were M = 8.06 and M = 6.9, respectively; and the adiabatic index γ was set equal to 1.35, roughly the average of the real-air values over the range of physical temperatures and pressures encountered in these calculations.

Results are shown in Figs. 3 - 6. Figure 3a displays calculated density contours after 1000 timesteps for an incident shock I arriving from the right with $\theta_w = 20^{\circ}$, and M = 6.9, a case for which complex Mach reflection results (Cf. Fig. 2). The incident shock I, the Mach stem M_1, the slip or contact surface CS, and R and R´, the shocks reflecting from the wedge and the first Mach stem, respectively, are marked. The fanlike lines labeled M_2 have been added where the density is steepening up, suggesting the system is close to developing a second Mach shock. The contour levels are identical with those chosen by Ben-Dor [10] in processing his interferogram data (Fig. 4a).

Figure 3b displays calculated density contours after 800 timesteps for the case with $\theta_w = 26.56^\circ$ and $M = 8.06$. The structure obtained is characteristic of double Mach reflection. The incident shock I, the Mach stems M_1 and M_2, the contact surface CS, and R and R´ are marked.

By comparing Figs. 3a and 4a, we see that not only the shape of the reflected wave fronts, but also the calculated contour levels interior to them are in excellent quantitative agreement with their measured counterparts. Figure 4b displays the calculated density and pressure profiles along the wedge for this case, showing the steep jump at the position of the Mach stem M_1 and the locations of the two maxima.

In Fig. 5 the pressure calculated on the wedge is plotted and compared with Ben-Dor's [10] experimental data. The discrepancies are concentrated in the two pressure peaks, both of which lie substantially above the measurements. There are two explanations for this: (1) at high temperatures, the effective value of γ in real air drops (see Section IIIC), reducing the pressure jump across a shock; and (2) Ben-Dor's data were apparently less well resolved than the numerical results (or possibly the peaks were eroded in the course of his data reduction).

Figure 6 shows an expanded view of the flow field in the neighborhood of the region where the contact surface approaches the wedge. Each line segment denotes the magnitude and direction of the velocity defined at the point it is directed away from. The velocities are viewed in the reference frame moving with the first Mach stem; M_2 and CS have the same meanings as before. The slip line has been extended by following the flow markers. The "jelly-roll" effect is very pronounced; two complete circuits can be

distinguished. The ability to resolve such structures is largely responsible for the relative efficacy of FCT algorithms in solving this kind of problem.

All of the calculations on reflections from small-angle wedges carried out with the Leapfrog-Trapezoidal code utilized uniform mesh spacing with $\delta x = \delta y$. The meshes used extended up to 150 x 30 in size. Typical running times for 10^3 cycles were ~ 270 s, i.e., ~ 60 μs per cell-cycle.

B. Large Wedge Angles

As the wedge angle increases (i.e., as the incident shock strikes the reflecting surface more nearly normally), the opening angle α decreases. When it goes to zero, we have regular reflection (region RR of Fig. 2). However, if α is small but finite, then, as was explained in Section IIB, resolution of the Mach reflection region is impractical unless a regridding algorithm is employed. The dynamic regridding procedure of FAST2D was used for this purpose in two calculations: $\theta_w = 44^\circ$, M = 5.074, and $\theta_w = 46.5^\circ$, M = 5.046, both with the real air EoS. These cases are indicated with open circles in the double Mach reflection region of Fig. 2. Note that, in contrast with the small-wedge-angle cases, they correspond to detached reflection. Our boundary conditions are inconsistent with detachment, but this should not affect the veracity of the calculated solution away from the corner of the wedge.

Figure 7 shows pressure contours from four different times in the 44° calculations. We have used enough contours to show the coarse structure but

require a larger number to resolve the feature corresponding to CS in Fig. 3. Only the finely-gridded portion of the mesh is shown in the figure. Little detail can be discerned in frames (a) and (b). By frame (c), M_1 is distinguishable; in frame (d), R, R', M_1, and M_2 are all well resolved. The contours in the first three frames, which were generated using an ideal-gas EoS, are sensibly identical with those at the corresponding times in the real-air EoS calculation used to obtain the last frame.

Figure 8 shows plots of the pressure loading on the wedge in orthographic projection at various times. The contours tend to sharpen up at later times as resolution improves; to this extent the expected self-similarity in the solution fails to materialize. In the final frame the leading Mach stem is about 10 cells high; to reach this stage it had to traverse the equivalent of 450 uniform grid points. Similar contours were produced in the 46.5° calculations.

Because the $\theta_w = 44^{\circ}$ and $\theta_w = 46.5^{\circ}$ cases are so similar, we discuss only the latter. The computed value of α for $\theta_w = 46.5^{\circ}$ is approximately 2.5° for a real-air EoS (with γ held constant at the value 1.35 we obtain $\alpha \approx 3.2^{\circ}$). Either value agrees with that measured to within the experimental error, $\sim 2^{\circ}$. In Fig. 9, we compare the calculated (using the real-air EoS) and measured values of the pressure at the surface of the wedge. The upper traces are pressure plots vs. positions at two times (the unit of time is arbitrarily designated to be μs, whereupon the distances in cm become determined). The lower traces are time histories at two stations used in the BRL experiments[11]. (If the wave evolution adhered exactly to the approximate similarity description, spatial profiles and time histories would be completely equivalent).

The agreement in the shapes of the profile is striking. The values of the lower pressure peak, corresponding to the Mach stem M_1, are nearly identical. The calculated value of the second pressure peak is 11% lower than the measured value, and thus is still within experimental uncertainty. The rise in the values of both peaks and the sharpening in detail from the first to the second plot probably has the same explanation in both cases, namely, improved resolution as the mach stem grows. That is, we believe that the experimental histories are at the limit of the resolution imposed by the finite size and time response of the pressure sensors, which play the same role as space and time truncation errors in the finite-difference approximation. Figure 10 shows the history of the peak pressure on the wedge, this time calculated for an ideal gas with $\lambda = 1.35$. The effect of improvement in resolution with increasing time is again apparent.

Figure 11 shows how well the double Mach reflection structure is resolved in the simulation. The pressure in bar is plotted along the trajectory pressure discontinuity (I, R', M_2, and the flow "stagnation" point on the boundary) in succession transversely. As can be seen, the pressure "discontinuities" are resolved equally well, within about 2 cells.

Movies have been made of the evolving density and pressure contours for the $\theta_w = 26.56^\circ$ and $\theta_w = 46.5^\circ$ cases, respectively, the various levels being identified by different colors. These movies (several frames from which are reproduced in Figs. 7 and 8) show graphically how the various features of the reflection structure sharpen up as sufficient resolution becomes available. They also show how efficiently the regridding algorithm moves to keep the reflection region in the finely gridded part of the mesh, tracking it smoothly without sudden or wide shifts.

The 46.5° movie demonstrates the slow development of the Mach structure and permits us to trace the locations of the pressure peaks along the wedge surface. The 26.56° movie uses Ben-Dor's density contours and clearly resolves

the Double Mach structure by permitting the structure to move twice as far along the wedge as in the above test calculations. This capability results directly from our use of the adaptive regridding algorithm.

C. Code Comparisons

A number of trial calculations were performed during the process of code development in order to test the boundary and initial conditions, EoS routine, etc. More critical test runs were carried out to compare the Leapfrog-Trapezoidal and FAST2D codes under identical conditions, and to determine the effect of using the real-air EoS instead of the ideal-gas EoS.

For the former test we started with the results obtained by the Leapfrog-Trapezoidal code for a Mach number $M = 8.06$ and wedge angle $\theta_w = 25.56^o$, using an ideal-gas EoS with $\gamma = 1.35$. Then we ran the same problem using FAST2D with a uniform mesh, disabling the regridding procedure and setting the timestep equal to those employed in the earlier run. Figure 12 shows the resulting density contours, along with those obtained experimentally by Ben-Dor.[10] Comparisons of the results at identical time levels up to cycle 800 yielded the following conclusions:

(1) The two codes yielded qualitatively (and in most respects quantitatively) similar results.

(2) Slip lines were better resolved by the Leapfrog-Trapezoidal code.

(3) The pressure calculated by the latter at the location of the wedge showed a greater tendency to numerical fluctuations (Fig. 2). The first pressure peak, just behind the leading Mach stem, was slightly higher in this calculation.

(4) An anomalously low (less than ambient) pressure was produced at one point by FAST2D because of timesplitting. This, however, had no apparent effect on the rest of the grid, nor did any discernible adverse consequences of timesplitting appear elsewhere.

To determine the role played by the real-air EoS, we repeated the FAST2D runs described earlier ($\theta_w = 44^o$, M = 5.074, and $\theta_w = 46.5^o$, M = 5.046) with constant $\gamma = 1.35$. (In order to obtain the same pressure jumps across the initial shock, the Mach numbers had to be adjusted to M = 5.173 and M - 5.148, respectively). Agreement with the BRL data was still good. At 1000 steps both pressure peaks in the 46.5^o case were too high in the ideal-gas calculation; the one at the Mach stem by ~10%, and that at the intersection of the slip surface with the wedge by ~11%. Similar results were observed in the 44^o calculations. The penalty for using the real-air EoS in its optimized vector form is about a 20% increase in running time.

IV. RELATED CALCULATIONS

Several additional calculations were performed which bear closely on the airblast problem: a shock reflecting from a wedge in a reactive medium, and preliminary height-of-burst (HoB) calculations.

A. Reflecting Shock in a Reactive Medium

Under a Navy-supported program to study combustion hydrodynamics, LCP has developed a simple numerical treatment of combustion processes based on the induction time hypothesis.[12] This model represents the chemistry through a composite process, in which reactants begin to combine into combustion products only after a finite "induction" time has elapsed. The rate at which the energy-releasing reactions proceed depends upon a single parameter, the induction time. This in turn is a function of the local thermodynamic variables.

As part of the LCP Combustion Hydrodynamics project, we have applied the induction time hypothesis model to study shock reflections in reactive gases (stoichiometric mixtures of H_2 in air or oxygen) at low pressure (0.1 atm). Figure 13 shows the time development of a detonation initiated by a weak reflecting shock in an H_2-air mixture. The sequence of six pressure contour plots traces the evolution of a detonation wave initiated by complex Mach reflection at the surface of the wedge. The incident shock was chosen so that the pressure behind it is too low to cause detonation to take place within the time of the calculation. As with the calculations of Section III, we have used open boundary conditions at the sides and top of the system.

Figure 13a shows the pressure contours corresponding to an incident shock with $\theta_w = 25^o$ and M = 4.0 (giving rise to complex Mach reflection) which has just begun to reflect. The Mach stem is initially too small to be resolved. In frame b, the Mach stem becomes discernible, but as yet no apparent reaction has occurred. By frame (c) the material has begun to ignite at a position well behind the current location of the Mach stem. When the Mach stem passed that position the pressure increase heated the mixture sufficiently to cause ignition after a short induction time characteristic of the H_2 -- air mixture. In frames (d) and (e), at later times, the pressure at the Mach stem continues to grow, leading to shorter characteristic induction times for material between the Mach stem and the original ignition point. Thus, we see the ignited region accelerate along the wedge surface toward the Mach stem. Because more energy is being released as the burning continues, the boundary of the ignited region also accelerates in the direction of the reflected shock and Mach stem, as we see from the decrease in the separation of the pressure contours near both locations. A stable detonation pattern has not yet emerged, however. This is evident from the bending out of the Mach stem and the lower density of contours between the Mach stem and the reflected shock/detonation front.

A similar calculation has been carried out in which all four boundaries were made reflecting. This is seen to be subcritical, i.e., a stable detonation wave does not form. When the incident shock Mach number is increased to M = 5.0, however, a stable detonation wave does occur. As it evolves, an intricate pattern of multiple reflections from the boundaries develops. Color movies have been made of the pressure contours for both calculations, illustrating clearly the difference in the two physical situations.

These studies have led to the discovery of previously unreported pockets of unreacted gas which become folded in behind the oscillating cellular multidimensional structure which characterizes most real detonations. These pockets, which react eventually some time after the main shock and reaction zone have passed, ought to be experimentally observable. They also may prove to be the mechanism by which detonations sustain themselves at abrupt area changes and in free space where there are no walls to provide new cellular detonation centers.

B. Height-of-Burst Calculations

FAST2D is written in such a way as to permit switching from Cartesian to cylindrical geometry by changing a single input parameter. A sample HoB calculation was carried out by introducing a 1 kg explosive charge at a height of 7.5 cm approximately reproducing the conditions of the Mighty Mach experiments. The resulting blast wave is initially spherical (i.e., semicircular when projected on the r-Z half plane; see Fig. 14). By using vertically stretched cells at the top of the mesh, it is possible to prevent the blast wave from reflecting back into the ground reflection region until late in the development of the expanding shocked system.

Unlike the constant-strength incident shocks discussed previously, the pressure (or density, etc.) profile through the front varies temporally in two ways: it weakens due to spherical expansion, and it steepens and narrows because the subsequent rarefaction wave tends to catch up with the shock. A third effect contributes significantly to time variation in real airblasts produced by high explosives: the delayed combustion of the HE charge.[13] This could be properly treated using a simple model like that based on the induction induction time hypothesis (Section IV A), and a turbulent mixing model, coupled with an accurate EoS for the detonation products. The present calculation neglected the effect of the delayed energy release,which will be included in the future.

Because the incident wave structure differs in both space and time from that assumed in the shock-on-wedge problems, the reflected wave now looks very different (Fig. 15). The Mach stem M_1 is still visible, but the rarefaction wave prevents the formation of a second Mach shock and distorts the reflected wave and contact surface.

Finally, as an example of what can be done with the computational tools in hand, we performed a HoB calculation with a ground structure. The latter was a block having a front face sloping at 45° (Fig. 14). Reflecting boundary conditions were employed on the structure, with the ramp modeled by a stair-step boundary. In addition to contour plots like those previously described, pressure histories were obtained at four locations along the ramp (Fig. 16). The traces on the left in Fig. 16 represent time histories of the maximum (as a function of horizontal position) pressures on the mesh at the elevations corresponding to sensors 1, 2, 3, 4, respectively, showing that these increase with elevation. It is interesting to note that the highest peak pressure on the structure was recorded at location 2, not at the bottom of the ramp.

REFERENCES

1. Boris, J. P., and Book, D. L., "Flux-Corrected Transport: I. SHASTA, A Fluid Transport Algorithm that Works," J. Comp. Phys. 11, 38 (1973).

2. Book, D. L., Boris, J. P., and Hain, K., "Flux-Corrected Transport: II. Generalizations of the Method," J. Comp Phys. 18, 248 (1975).

3. Boris, J. P., and Book, D. L., "Flux-Corrected Transport: III. Minimal-Error FCT Algorithms," J. Comp. Phys. 20, 397 (1976).

4. Boris, J. P., and Book, D. L., "Solution of Continuity Equations by the Method of Flux-Corrected Transport," in Methods of Computational Physics, Vol. 16, Ed. by J. Killeen (Academic Press, New York, 1976).

5. Zalesak, S. T., "Fully Multidimensional Flux-Corrected Transport Algorithms for Fluids," J. Comp. Phys. 31, 335 (1979).

6. Zalesak, S. T., "High Order "ZIP" Differencing of Convective Terms," NRL Memorandum Report No. 4218 (1980).

7. Book, D. L., Boris, J. P., Kuhl, A. L., Oran, E. S., Picone, J. M., and Zalesak, S. T., "Simulation of Complex Shock Reflections from Wedges in Inert and Reactive Gaseous Mixtures," Stanford, CA, 23-30 June 1980, Proceedings of the Seventh International Conference on Numerical Methods, (Springer-Verlag, New York, to be published).

8. Boris, J. P., "Flux-Corrected Transport Modules for Solving Generalized Continuity Equations," NRL Memorandum Report No. 3237 (1970).

9. Kuhl, A. L. (personal communication); adapted from Lawrence Livermore Laboratory, Report No. UCRL 51892 (1979); NRL version optimized by T. R. Young, Jr.

10. Ben-Dor, G., "Regions and Transitions of Nonstationary Oblique Shockwave Diffractions in Perfect and Imperfect Gases," University of Toronto Institute of Aerodynamic Studies, Report No. UTIAS 232 (1978); see also Ben-Dor, G., and Glass, I. I., "Domain and Boundaries of Nonstationary Oblique Shockwave Reflections: 1. Diatomic Gas," J. Fluid Mech. 92. 459 (1979).

11. Bertrand, B. P., "Measurement of Pressure in Mach Reflection of Strong Shockwaves in a Shock Tube," Ballistic Research Laboratories Report No. BRL-MR-2196 (1972).

12. Oran, E. S., Young, T. R., Jr., and Boris, J. P., "Application of Time-Dependent Numerical Methods to the Description of Reactive Shocks," Proceedings Seventeenth Symposium (International) on Combustion (The Combustion Institute, Pittsburgh, (1979).

Table 1

CODE	MACH NO.	WEDGE ANGLE	TYPE OF SHOCK	E.O.S. γ =	REZONE	# STEPS	EXPERIMENT
L-T	6.9	20°	CMR(A)	1.35	NO	1,000	BEN-DOR
L-T	8.06	26.56°	DMR(A)	1.35	NO	800	BEN-DOR
FAST2D	8.06	26.56°	DMR(A)	1.35	NO	800	BEN-DOR
FAST2D	5.173	44°	DMR(D)	1.35	YES	600	BRL
FAST2D	5.074	44°	DMR(D)	REAL AIR	YES	1,000	BRL
FAST2D	5.148	46.5°	DMR(D)	1.35	YES	1,000	BRL
FAST2D	5.046	46.5°	DMR(D)	REAL AIR	YES	1,500	BRL

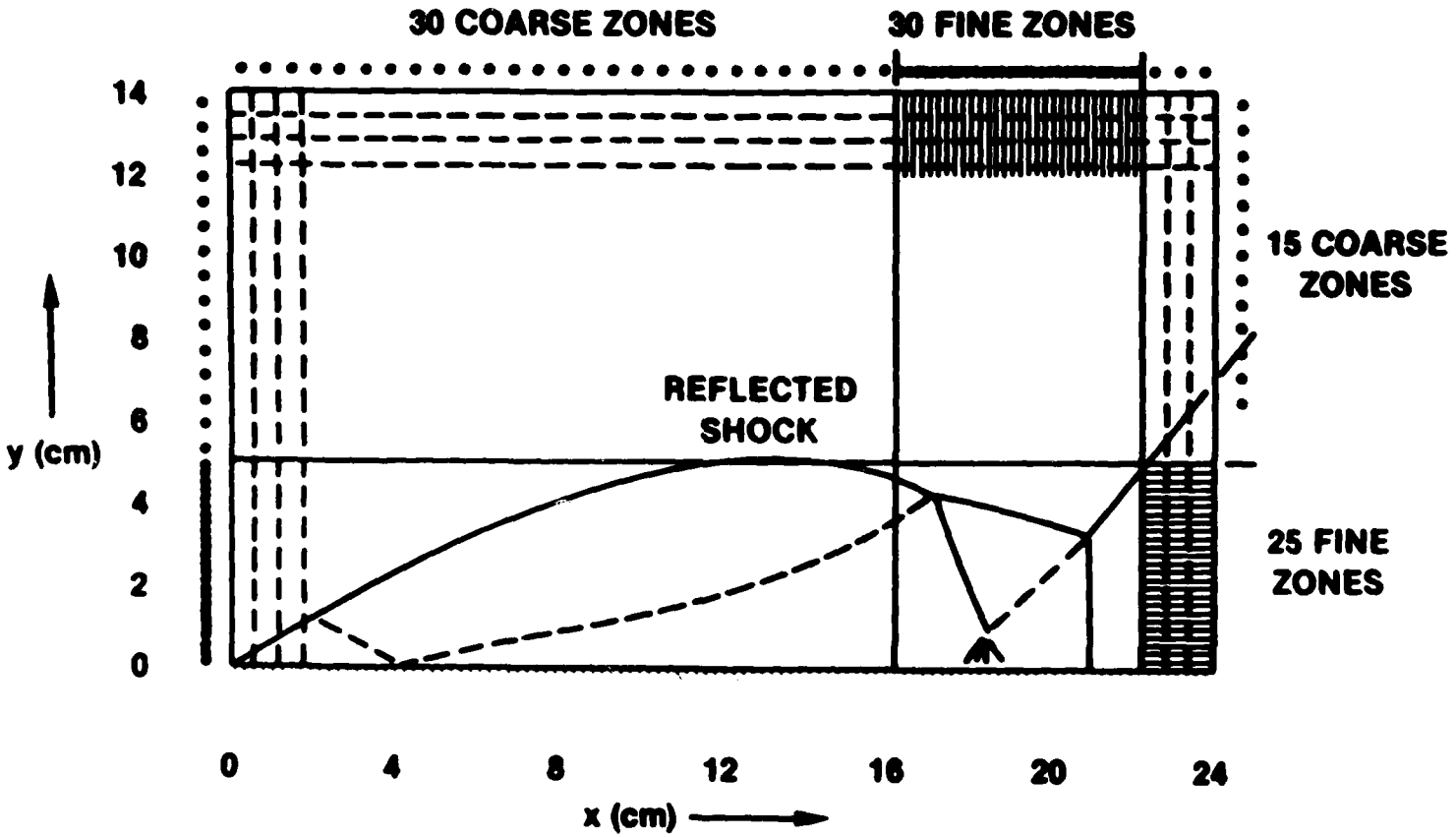

Fig. 1 - Gridding for complex shock reflection problem used in FAST2D code. Shown schematically are incident, reflected and Mach shocks (solid lines) and slip surfaces (broken lines) for incident shock arriving from the left. The finely gridded region moves with Mach stems and triple points to provide resolution where it is needed most.

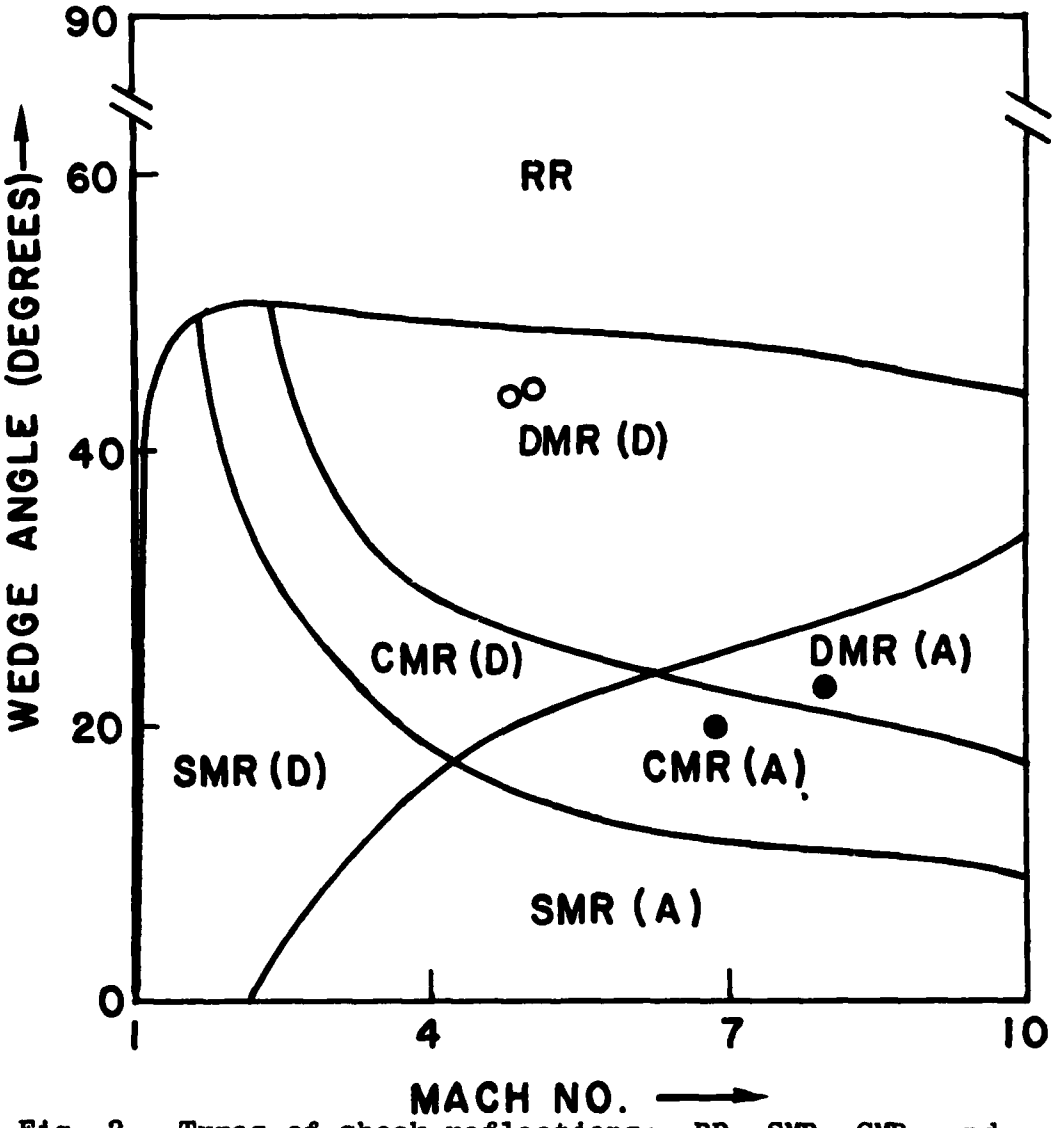

Fig. 2 - Types of shock reflections: RR, SMR, CMR, and DMR denote regular reflection and single, complex and double Mach reflection, respectively. D and A label detached and attached shocks, respectively. Closed circles represent calculations done with the Leapfrog-Trapazoidal code; open circles represent those done with FAST2D.

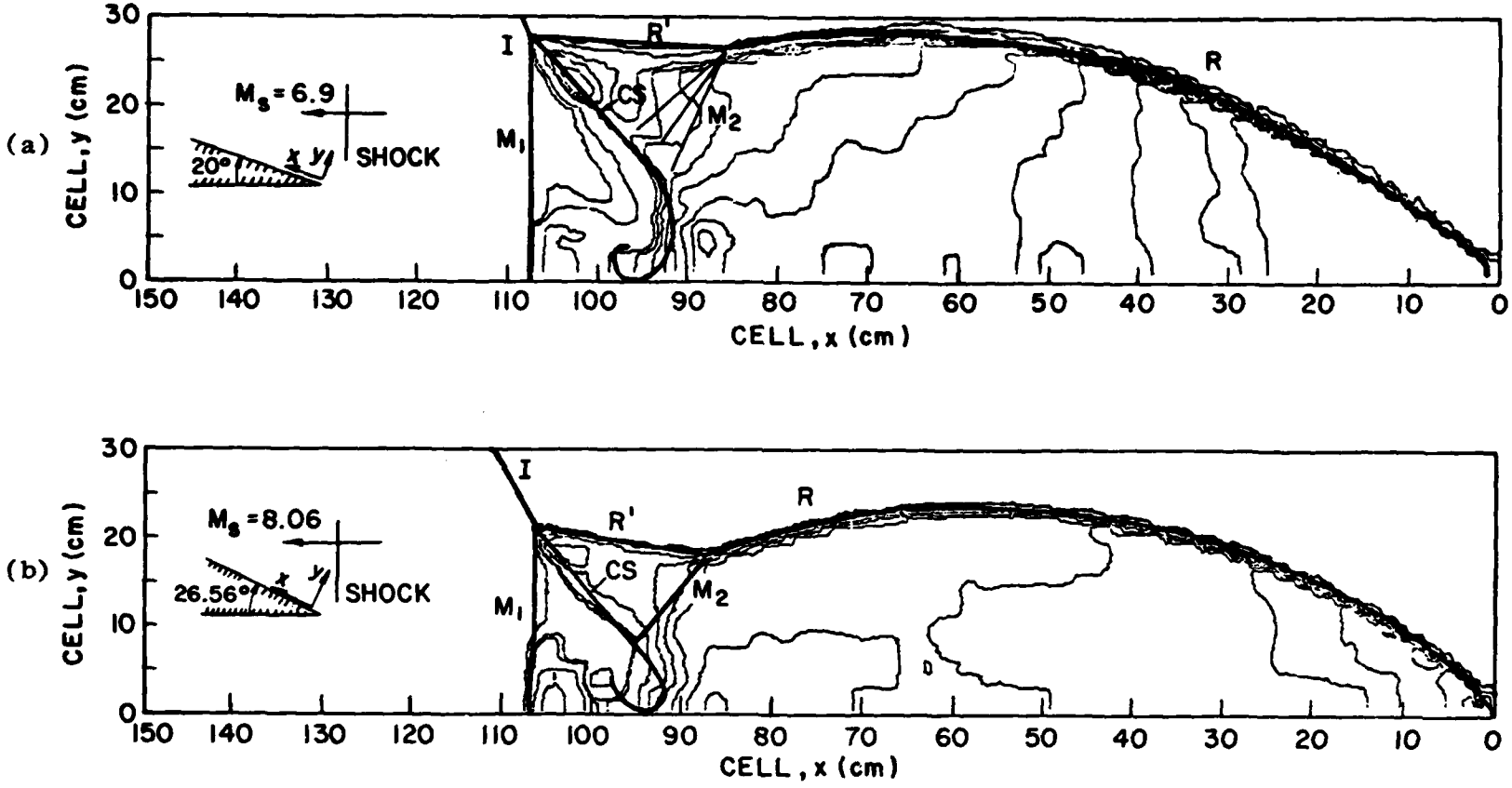

Fig. 3 - Wave structure and density contours with lines of discontinuity identified for (a) complex Mach reflection case ($\theta_w = 20^\circ$, M = 6.9); (b) double Mach reflection case ($\theta_w = 26.56^\circ$, M = 8.06).

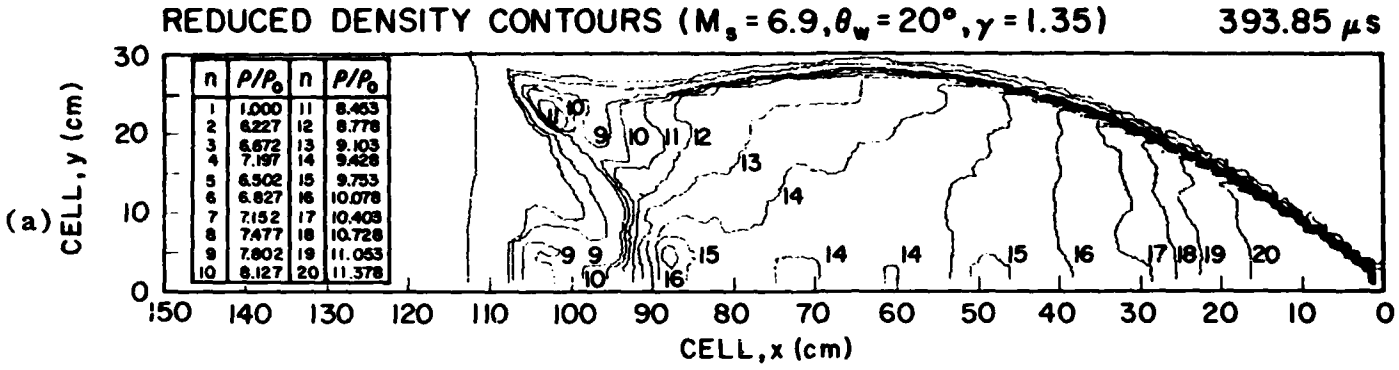

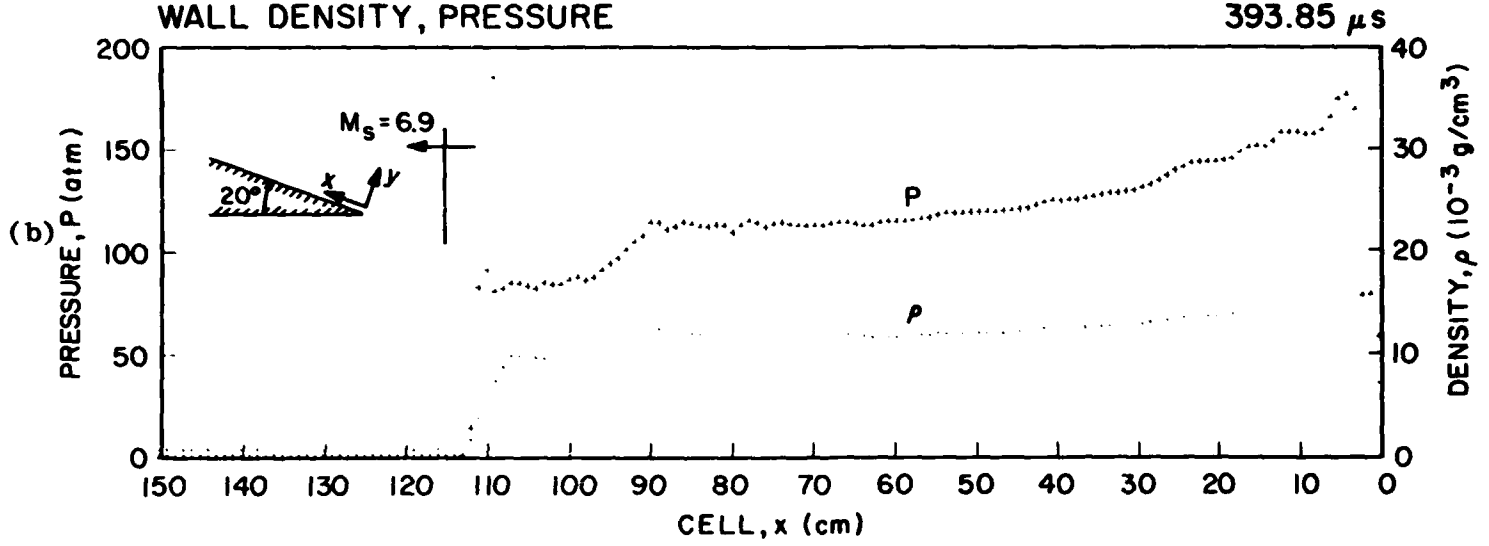

Fig. 4 - (a) Contours of Figure 3(a), labeled with density values used by Ben-Dor; (b) Density (dots) and pressure (plus sign) contours calculated on wedge (circles, fitted by solid line) and calculated value (dots).

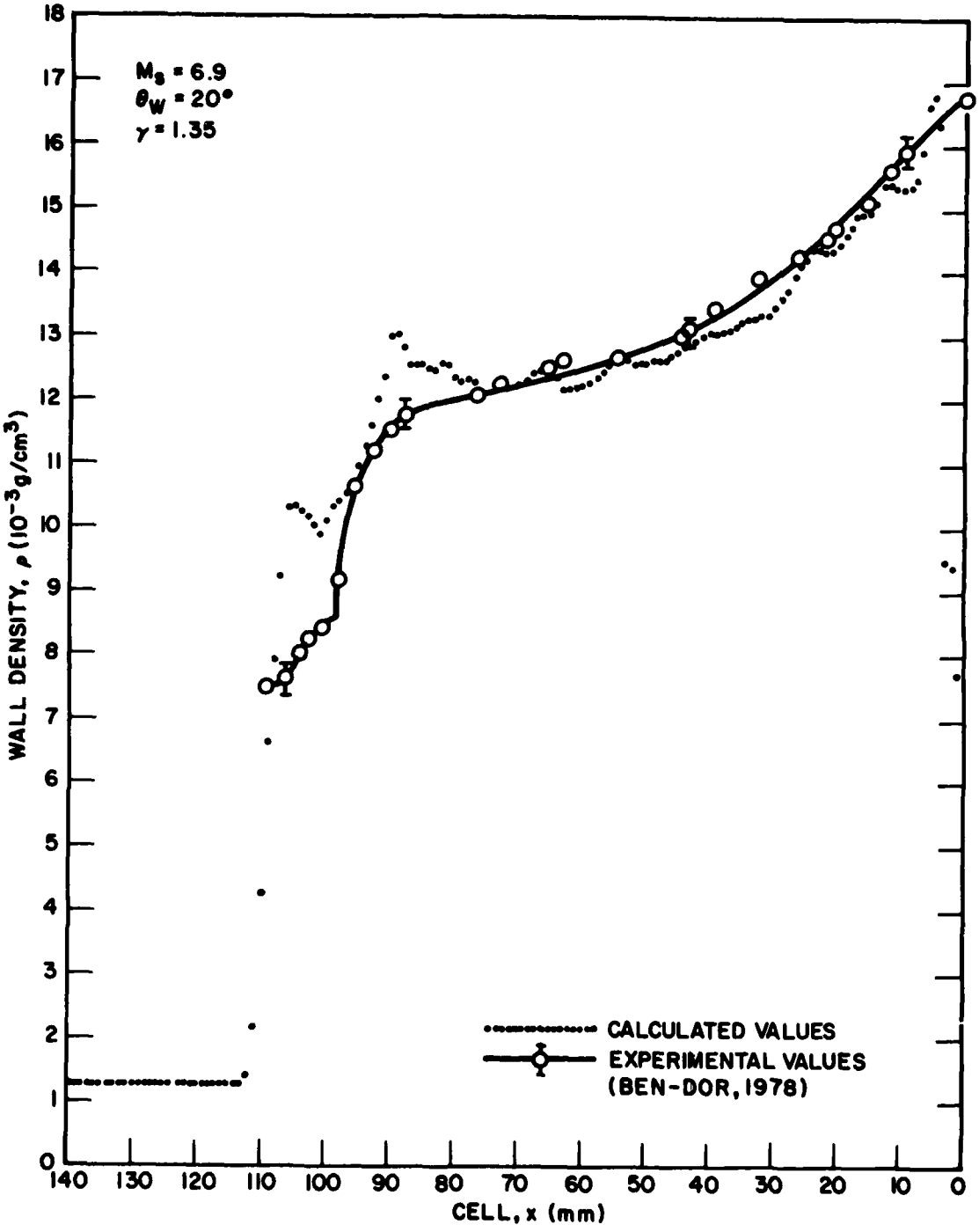

Fig. 5 - Comparison in complex Mach reflection case of experimentally measured density on wedge (circles, fitted by solid line) and calculated value (dots).

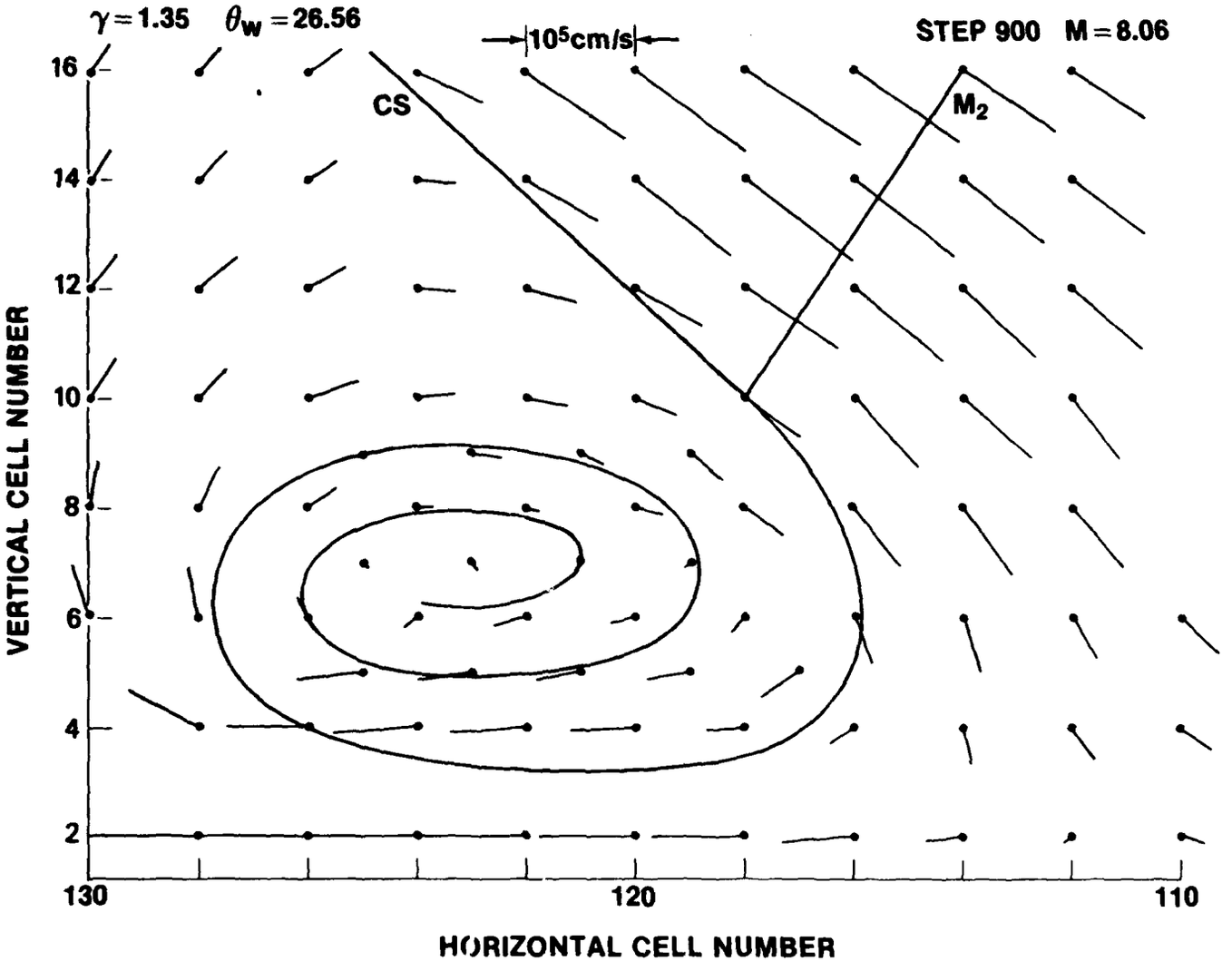

Fig. 6 - Rollup of slip line at wedge surface (solid line). Short line segments represent magnitude and direction of velocity at mexh points (dots), in reference frame of Mach stem.

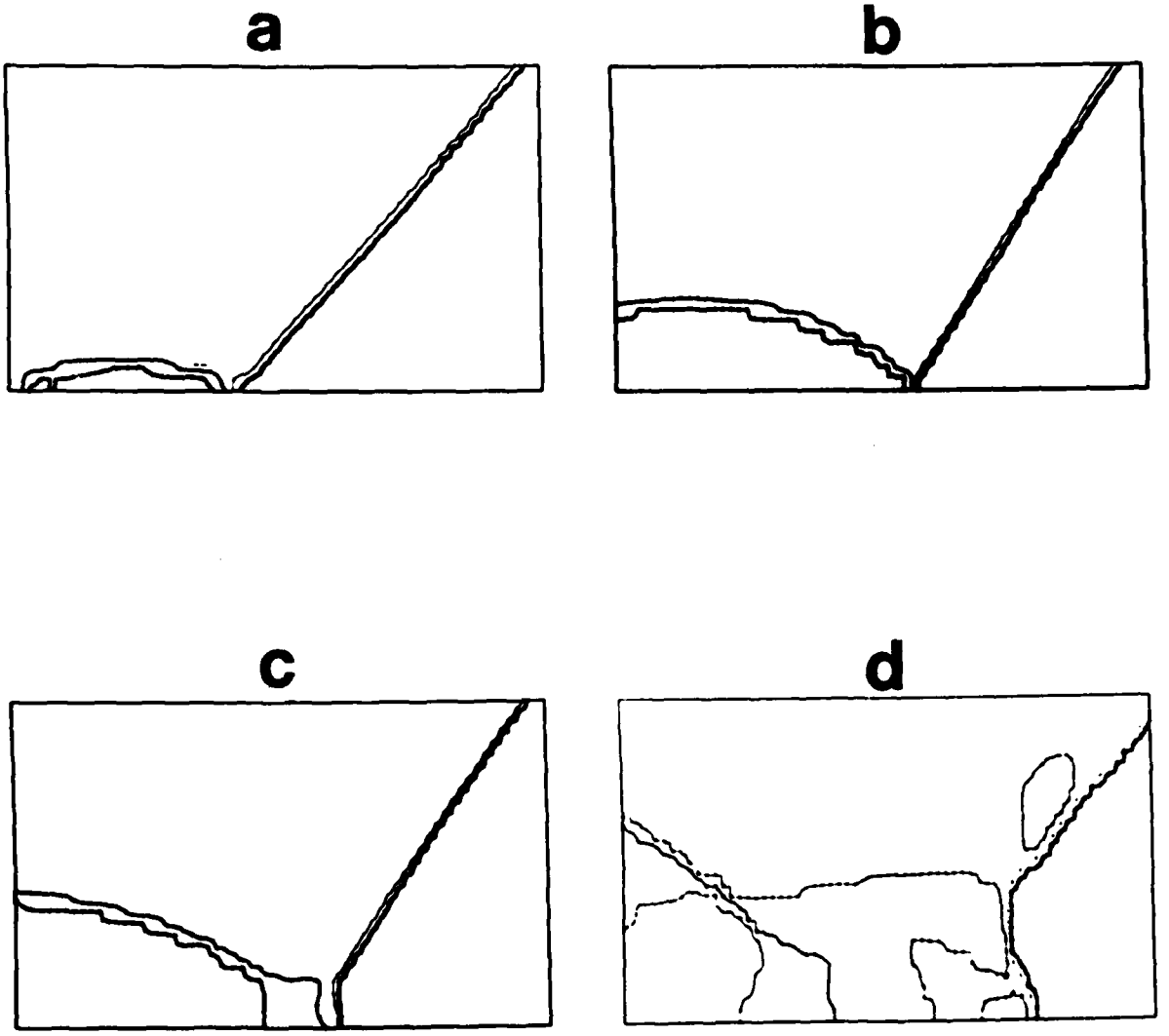

Fig. 7 - Development of Mach shock in ideal-gas 44-degree calculation. Pressure contours are shown at times (a) 1.57×10^{-5}; (b) 4.09×10^{-5}; (c) 5.95×10^{-5}; (d) 1.54×10^{-4} (this last frame taken from calculation using real air EOS).

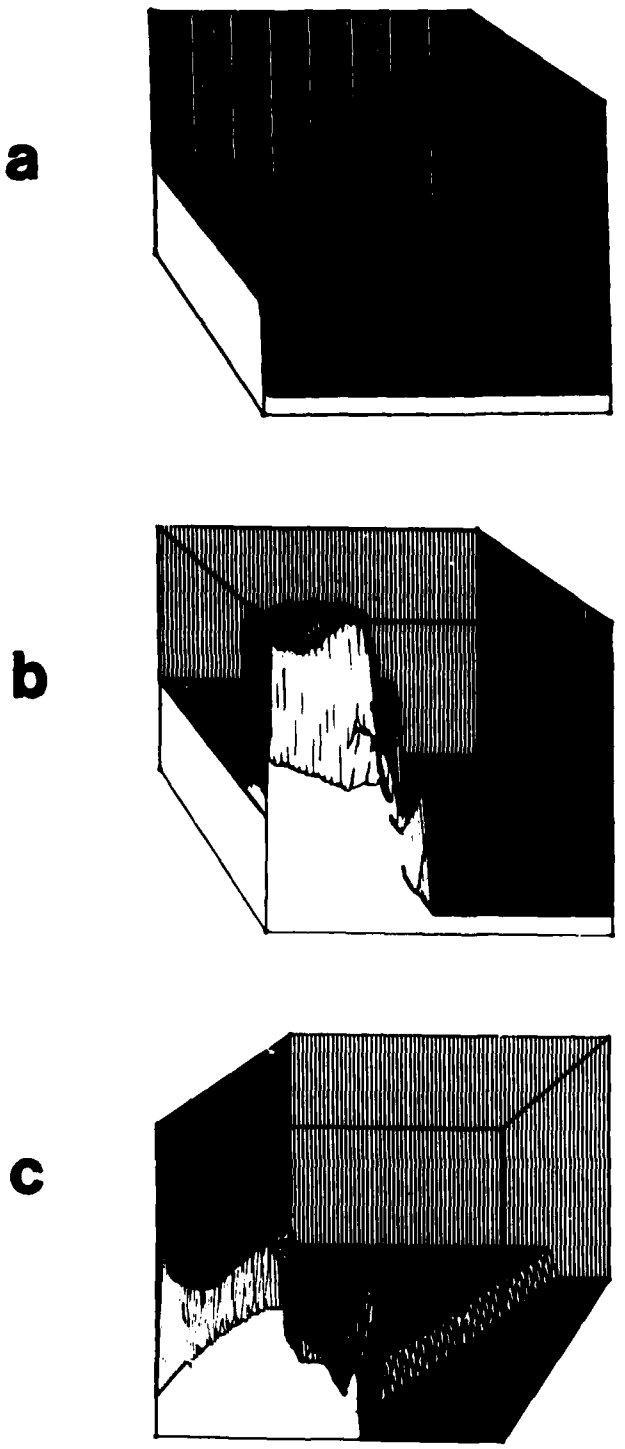

Fig. 8 - Pressure plots from ideal-gas 44-degree calculation in orthographic projection at times (a) 0.00; (b) 1.13 x 10^{-4}; (c) 1.60 x 10^{-4}; (taken from calculation using real-air EOS).

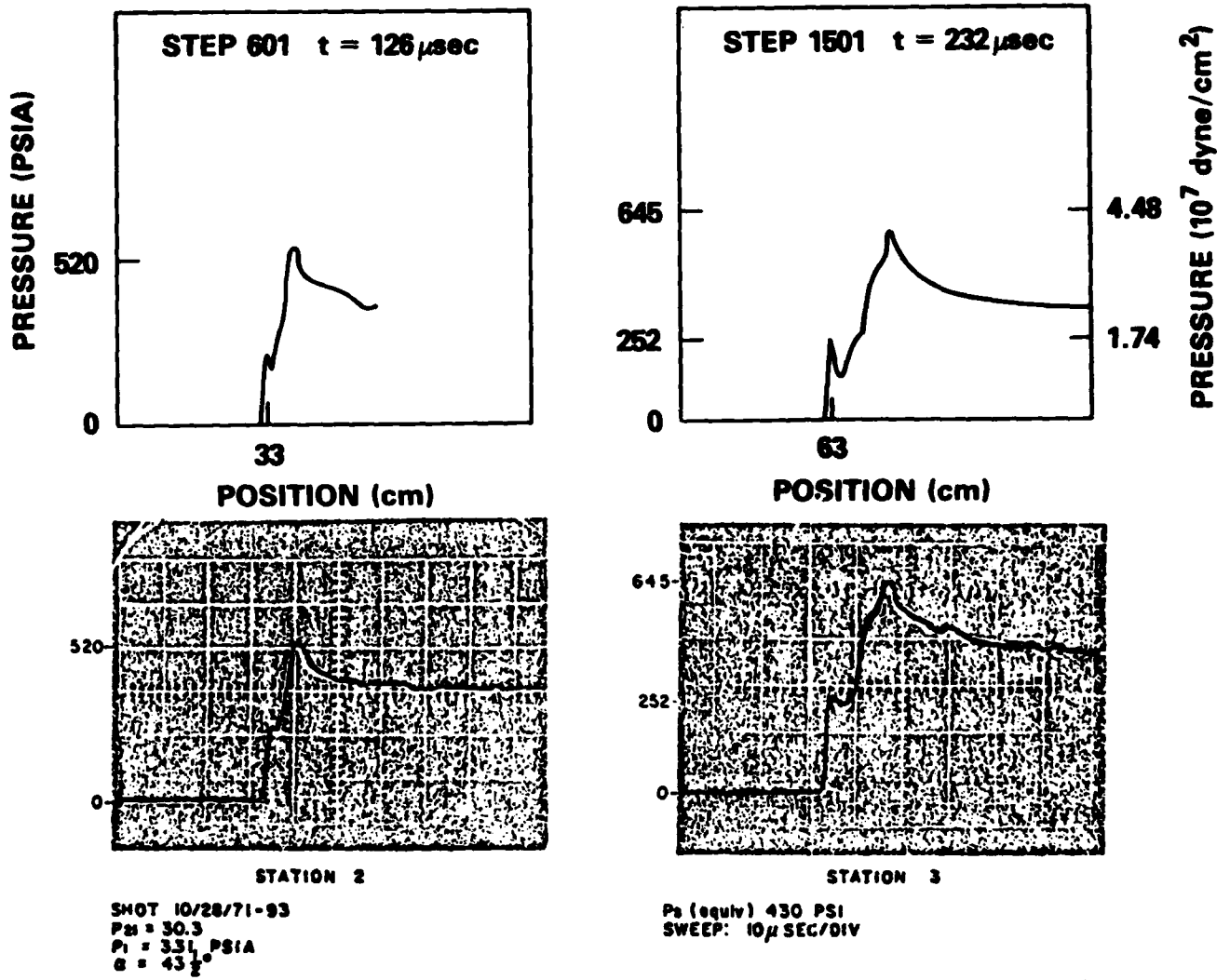

Fig. 9 - Upper and lower diagrams show pressure in PSIA on the wedge as a function of position for $\theta = 46.5^{o}$ (real-air EOS) at two times in the simulation (upper traces and at two stations in the BLR experiments [11] (lower traces).

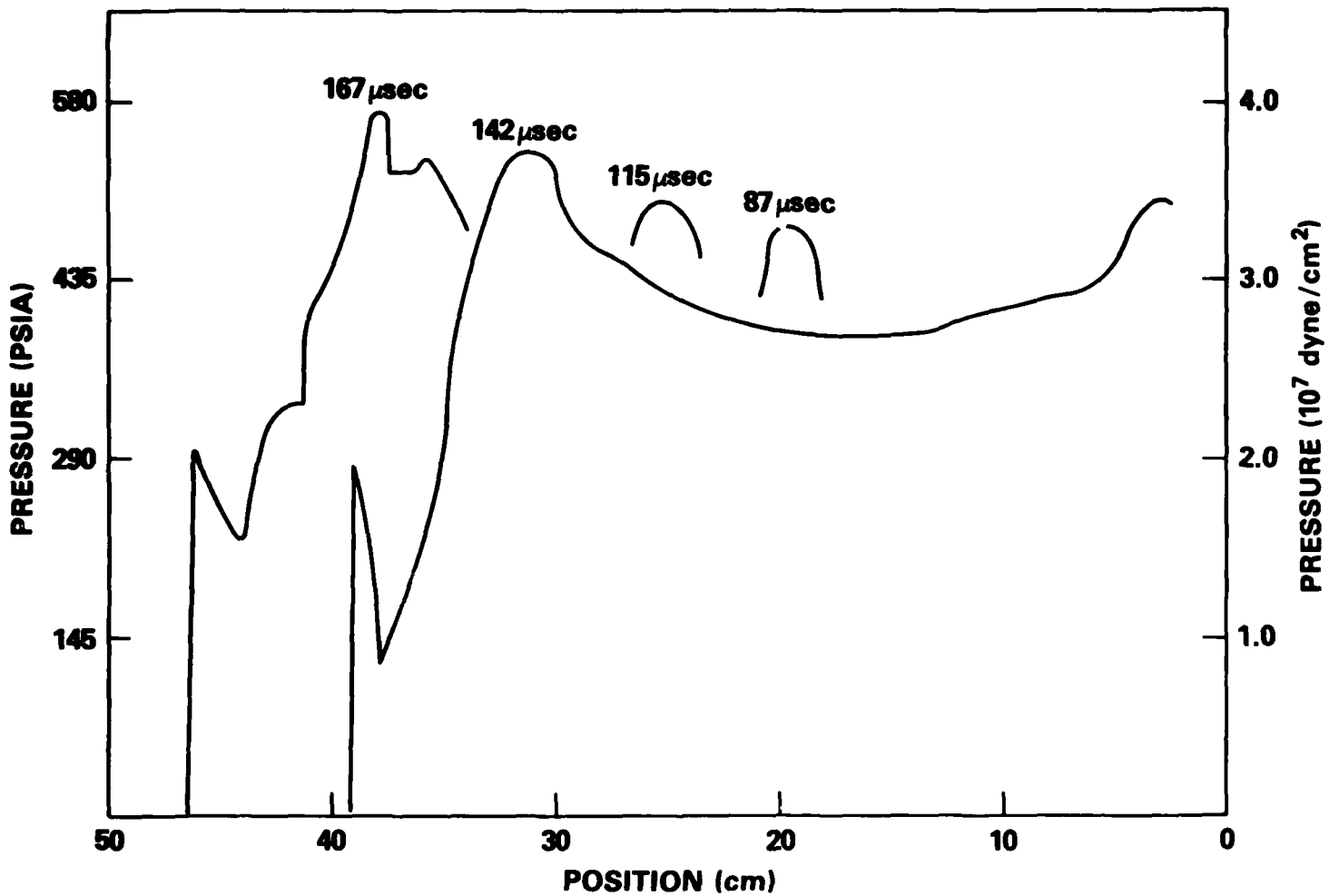

Fig. 10 - Pressure profile on wedge in 46.5° ideal-gas calculation at four different times, showing the effect of improving resolution.

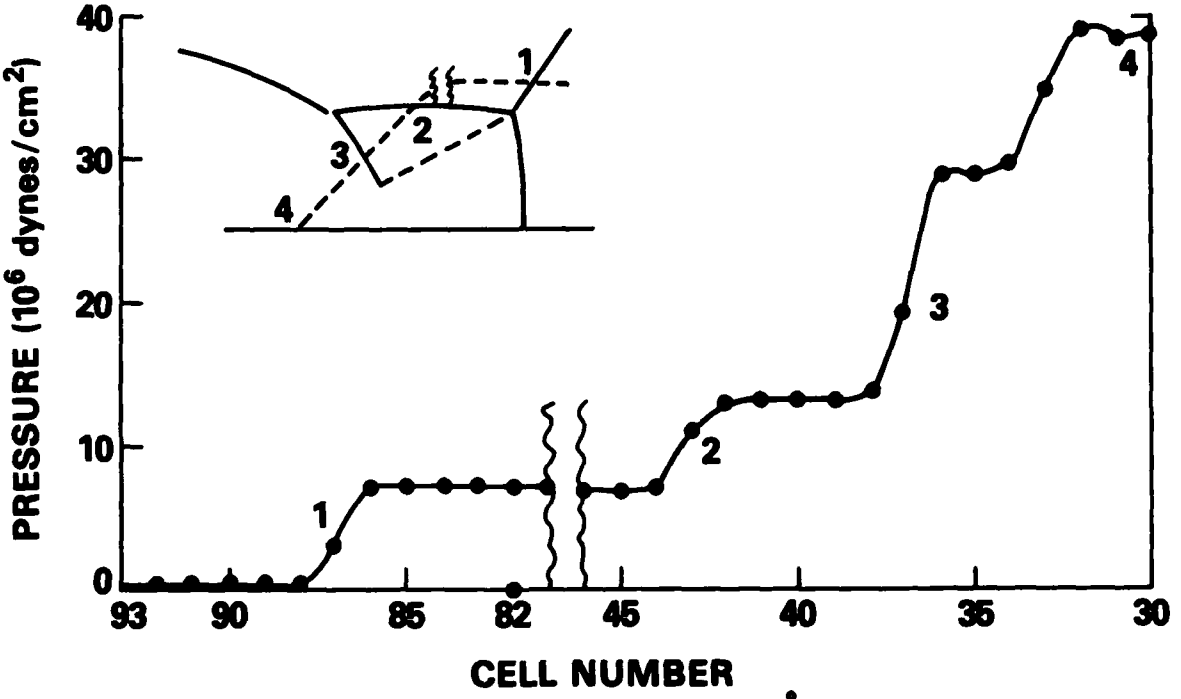

Fig. 11 - Plot of pressure vs position (46.5° wedge angle) along the trajectory 1-2-3-4 shown in the inset which intersects four surfaces of discontinuity (solid lines) transversely.

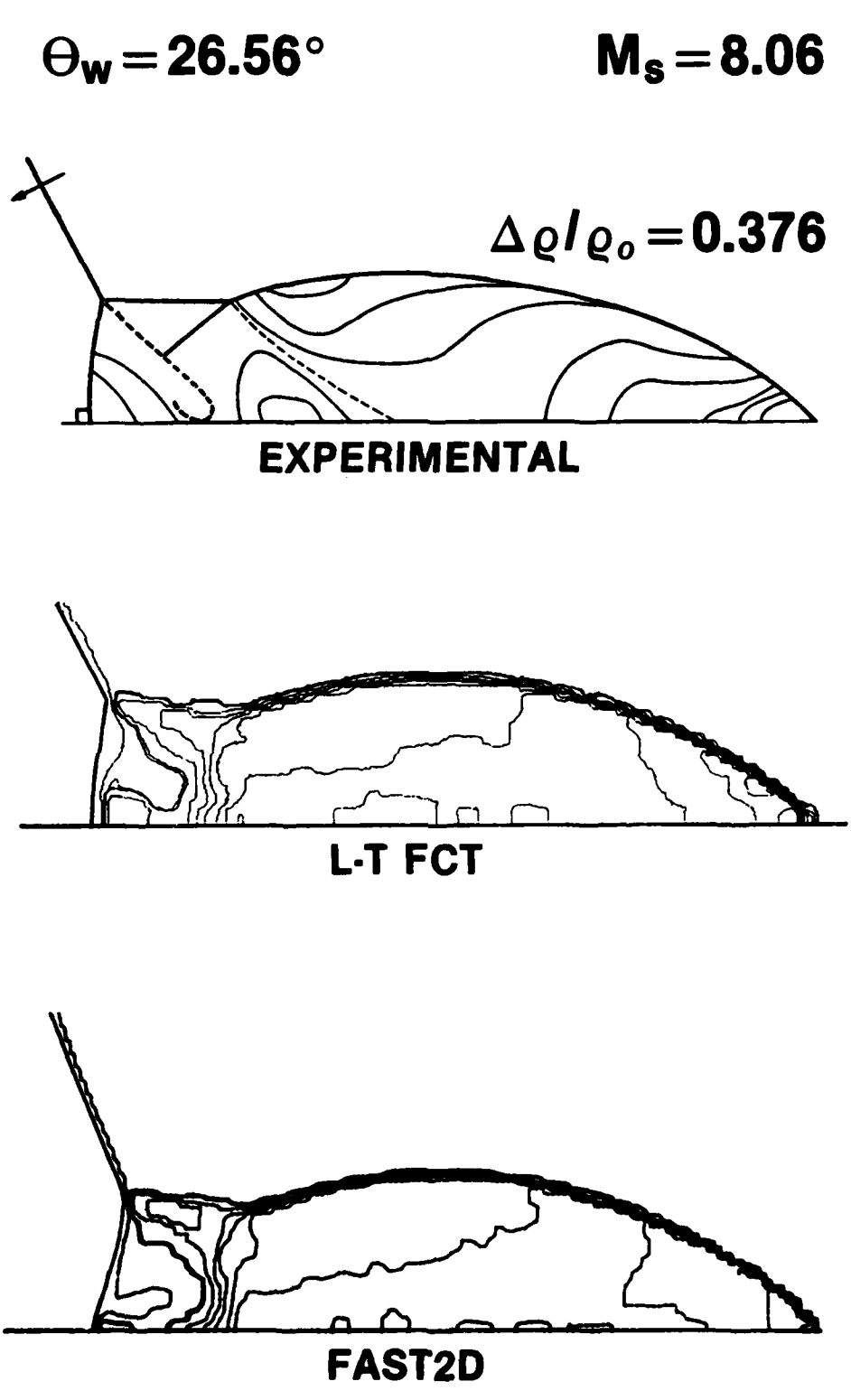

Fig. 12 - Comparison between experimental, Leapfrog-trapezoidal, and FAST2D double-Mach-reflection density contours.

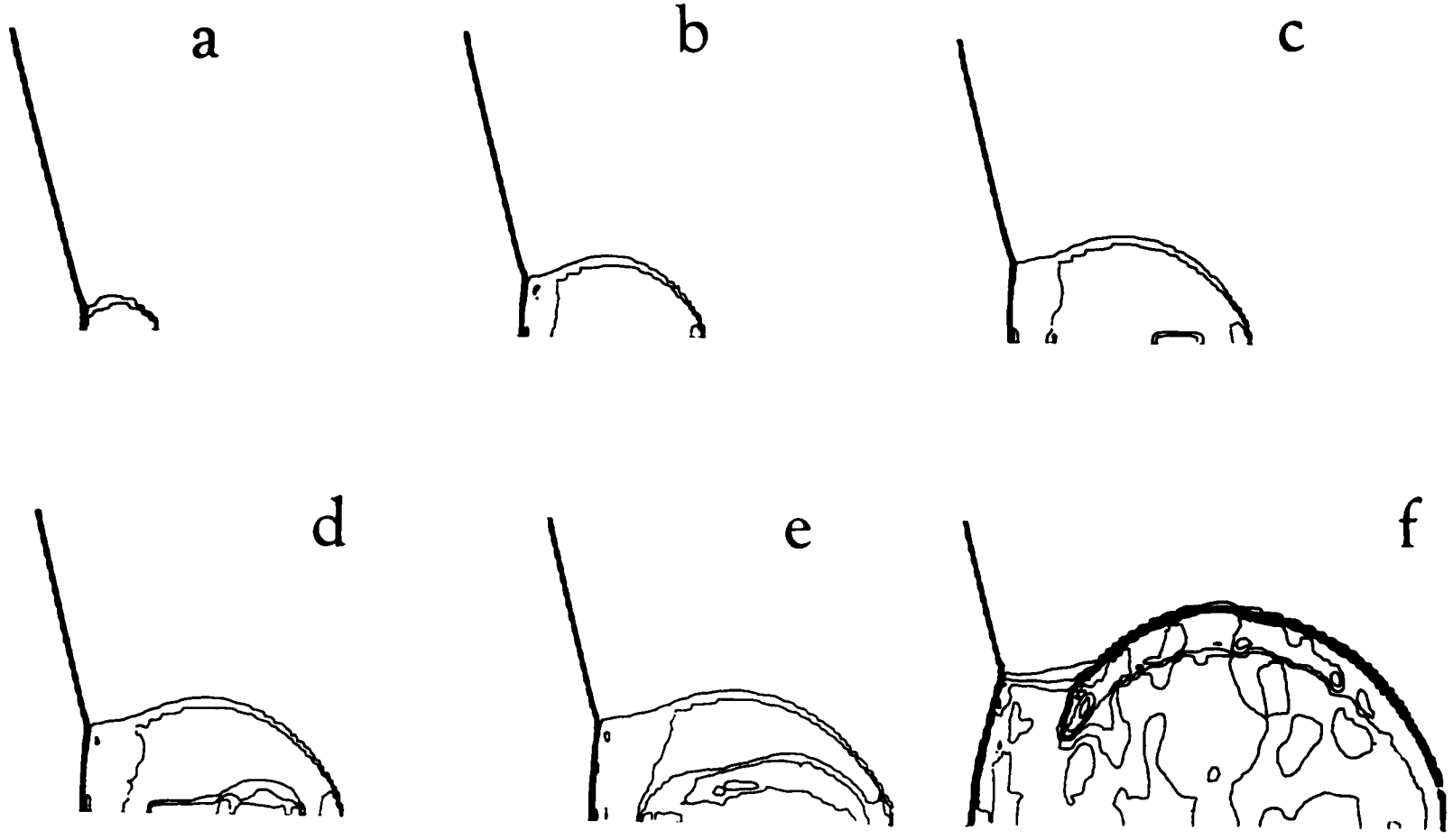

Fig. 13 - Pressure contours produced in detonation calculation (reflected shock in reactive medium) at times (a) 1.10×10^{-6} μs; (b) 2.70×10^{-6} μs; (c) 3.62×10^{-6} μs; (d) 3.91×10^{-6} μs; (e) 4.50×10^{-6} μs; (f) 6.73×10^{-6} μs.

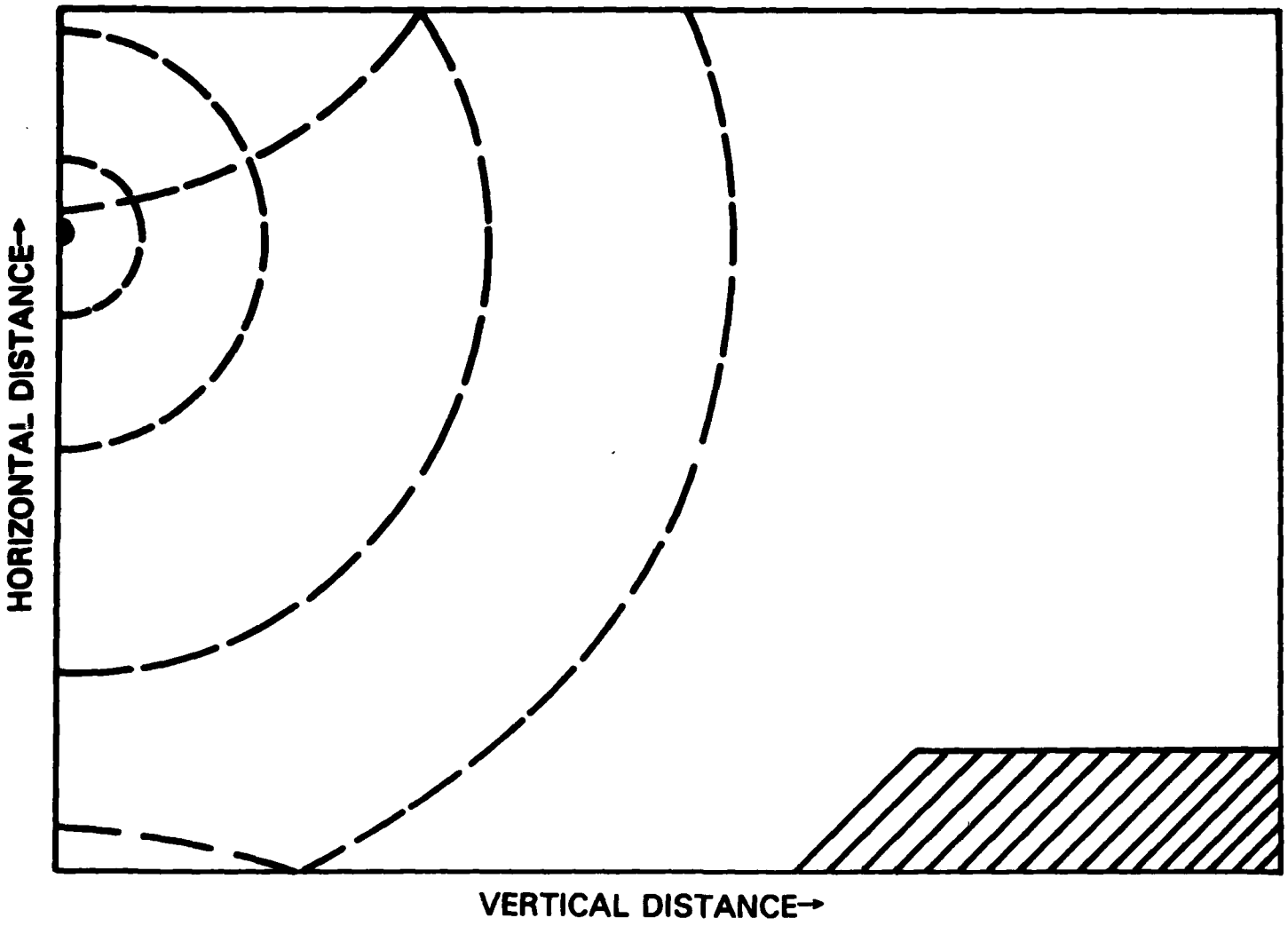

Fig. 14 - Schematic of HoB calculation. Energy release is at dot on vertical line (z axis). Shocks (dashed lines) reflect off boundaries, limiting the extent of validity in space-time of calculation. Hatched region indicates location of solid (reflecting) ground structure.

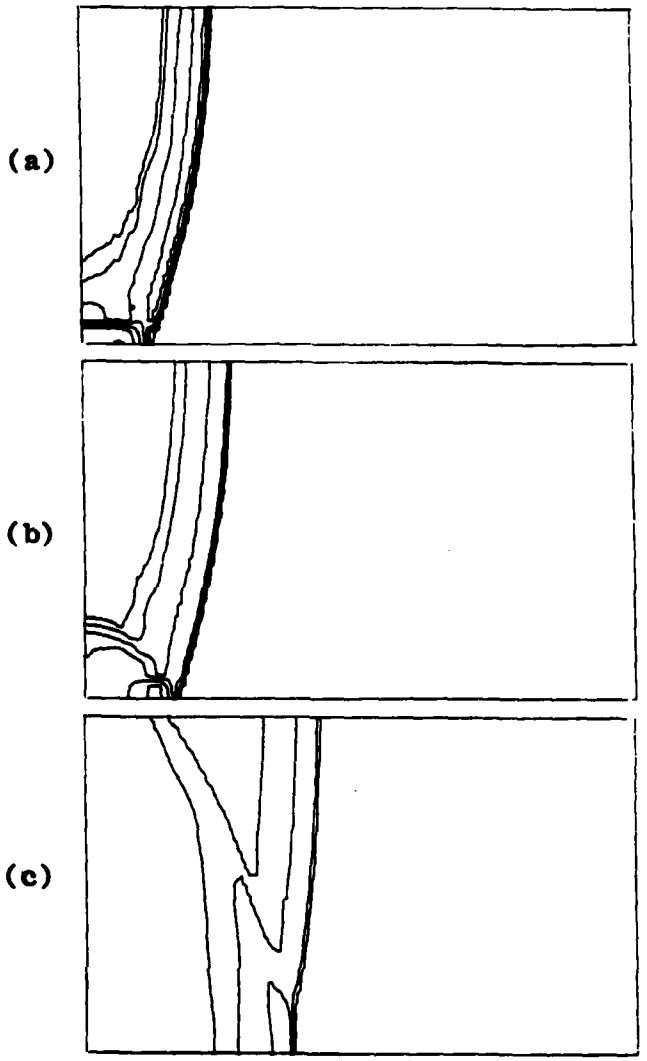

Fig. 15 - Development of Mach shock in HoB calculation. Pressure contours are shown at times (a) 5.70 x 10^{-5}; (b) 7.03 x 10^{-5}; (c) 1.62 x 10^{-4}.

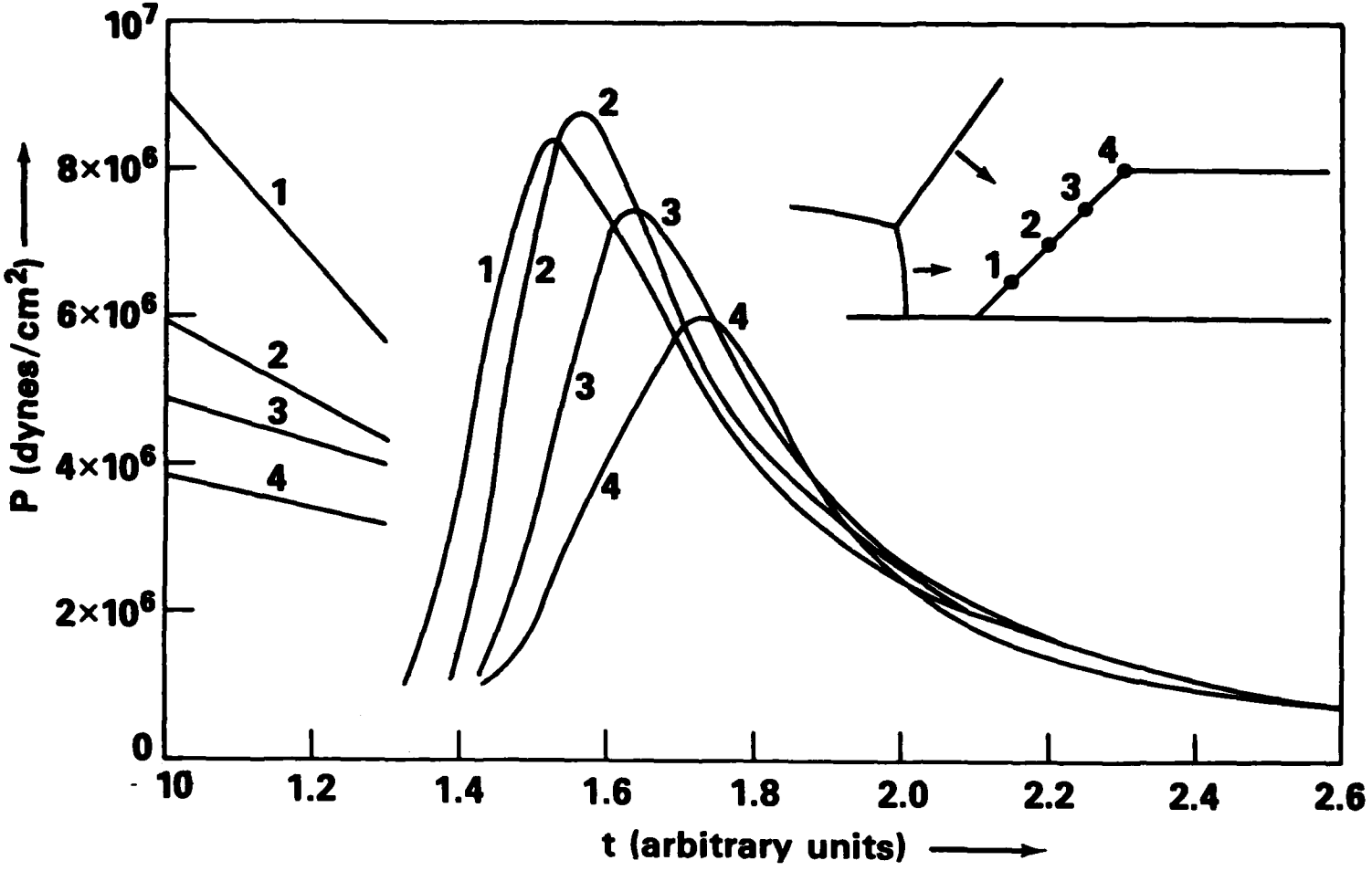

Fig. 16 - Pressure histories at four sensor locations on ramp of structure sketched in Figure 14.

DISTRIBUTION LIST

Assistant to the Secretary of Defense
Atomic Energy
Washington, DC 20301
Olcy Attn Executive Assistant

Director
Defense Advanced Rsch Proj Agency
1400 Wilson Blvd
Arlington, VA 22209
(desires only one copy to library)
Olcy Attn TIO

Director
Defense Communications Agency
Washington, DC 20305
(ADR CNWDI: Attn Code 240 for)
Olcy Attn Code 670 R LIPP

Director
Defense Intelligence Agency
Washington, DC 20301
Olcy Attn DB-4C E OFARREL
Olcy Attn DB-4N
Olcy Attn DT-1C
Olcy Attn DT-2
Olcy Attn RDS-3A (TECH LIB)

Director
Defense Nuclear Agency
Washington, DC 20305
02cy Attn SPSS
04cy Attn TITL
Olcy Attn DDST

Defense Technical Information Center
Cameron Station
Alexandria, VA 22314
(12 if open pub, otherwise 2 -
no WNINTEL)
12cy Attn DD

Chairman
Department of Defense Explo Safety Board
Rm 856-C
Hoffman Building 1
2461 Eisenhower Avenue
Alexandria, VA 22331
Olcy Attn Chairman

Commander
Field Command
Defense Nuclear Agency
Kirtland AFB, NM 87115
Olcy Attn FCTMOF
Olcy Attn FCT
Olcy Attn FCPR

Chief
Field Command
Defense Nuclear Agency
Livermore Division
P O Box 808 L-317
Livermore, CA 94550
Olcy Attn FCPRL

Director
Joint Strat TGT Planning Staff
Offutt AFB
Omaha, NB 68113
Olcy Attn DOXT
Olcy Attn JLA
Olcy Attn JLTW-2
Olcy Attn NRI-STINFO Library
Olcy Attn XPFS

Commandant
Nato School (Shape)
APO New York, NY 09172
Olcy Attn U.S. Documents
Officer

Under Secy of Def for Rsch &
Engrg
Department of Defense
Washington, DC 20301
Olcy Attn Strategic &
Space Systems (OS)

Director
BMD Advanced Technology Center
Department of the Army
P O Box 1500
Huntsville, AL 35807
Olcy Attn 1CRDABH-X
Olcy Attn ATC-T

Commander
BMD Systems Command
Department of the Army
P O Box 1500
Huntsville, AL 35807
Olcy Attn BMDSC-H N HURST

Chief of Engineers
Department of the Army
Forrestal Building
Washington, DC 20314
Olcy Attn DAEN-RDM
Olcy Attn DAEN-MCE-D

Deputy of Chief of Staff for
OPS & Plans
Department of the Army
Washington, DC 20310
Olcy Attn DAMO-NC

Commander
Harry Diamond Laboratories
Department of the Army
2800 Powder Mill Road
Adelphi, MD 20783
(CNWDI-Inner Envelope:
Attn: DELHD-RBH)
Olcy Attn Chief Div 20000
Olcy Attn DELHD-I-TL (Tech Lib)

Commander
U.S. Army Armament Material Readiness
Command
Rock Island, IL 61202
Olcy Attn MA Library

Director
U.S. Army Ballistic Research Labs
Aberdeen Proving Ground, MD 21005
Olcy Attn DRDAR-BLE J Keefer
O2cy Attn DRDAR-TSB-S (Tech Lib)
Olcy Attn DRDAR-BLT W Taylor
Olcy Attn DRDAR-BLV

Commander
U.S. Army Communications Command
Fort Huachuca, AZ 85613
Olcy Attn Technical Reference Div

Commander
U.S. Army Concepts Analysis Agency
8120 Woodmont Avenue
Bethesda, MD 20014
Olcy Attn MOCA-ADL (Tech Lib)

Commander
U.S. Army Engineer Center
Fort Belvoir, VA 22060
Olcy Attn ATZA

Division Engineer
U.S. Army Engineer Div Huntsville
P O Box 1600, West Station
Huntsville, AL 35807
Olcy Attn HNDED-SR

Division Engineer
U.S. Army Engineer Div Ohio River
P O Box 1159
Cincinnati, OH 45201
(Unclassified Only)
Olcy Attn ORDAS-L (Tech Lib)

Director
U.S. Army Engr Waterways Exper
Station
P O Box 631
Vicksburg, MS 39180
Olcy Attn WESSD G Jackson
Olcy Attn WESSA W Flathau
Olcy Attn J Strange
Olcy Attn WESSE L Ingram
Olcy Attn Library

Commander
U.S. Army Foreign Science & Tech Ctr
220 7th Street, NE
Charlottesville, VA 22901
Olcy Attn DRXST-SD

Commander
U.S. Army Material & Mechanics
Rsch Ctr
Watertown, MA 02172
(Address CNWDI: Attn:
Document Control for)
Olcy Attn Technical Library
Olcy Attn DRXMR J Mescall
Olcy Attn DRXMR-TE R SHEA

Commander
U.S. Army Material Dev & Readiness
CMD
5001 Eisenhower Avenue
Alexandria, VA 22333
Olcy Attn DRCDE-D L Flynn
Olcy Attn DRXAM-TL (Tech Lib)
Uncl only

Commander
U.S. Army Missile Command
Redstone Arsenal, AL 35809
Olcy Attn DRDMI-XS
Olcy Attn RSIC

Commander
U.S. Army Mobility Equip R&D CMD
Fort Belvoir, MD 22060
(CNWDI to Army Mat Dev
& Readiness Command)
Olcy Attn DRDME-WC (Tech Lib)

Commander
U.S. Army Nuclear & Chemical Agency
7500 Backlick Road
Building 2073
Springfield, VA 22150
(desires only 1cy to Library)
Olcy Attn Library

Commandant
U.S. Army War College
Carlisle Barracks, PA 17013
Olcy Attn Library

Commander
David Taylor Naval Ship
R&D CTR
Bethesda, MD 20084
(CNWDI only Attn
Mrs. M. Birkhead
Code 5815.61)
Olcy Attn Code L42-3
(Library)

Officer-in-Charge
Naval Construction Battalion Center
Civil Engineering Laboratory
Port Hueneme, CA 93041
Olcy Attn Code L51 S Takahashi
Olcy Attn Code L51 R Odello
Olcy Attn Code L08A (Library)

Commander
Naval Electronic Systems Command
Washington, DC 20360
Olcy Attn PME 117-21

Commander
Naval Facilities Engineering Command
Washington, DC 20390
Olcy Attn Code 09M22C (Tech Lib)
Olcy Attn Code 03T
Olcy Attn Code 04B

Headquarters
Naval Material Command
Washington, DC 20360
Olcy Attn MAT 08T-22

Commander
Naval Ocean Systems Center
San Diego, CA 92152
Olcy Attn Code 4471 (Tech Lib)
Olcy Attn Code 013 E Cooper

Superintendent
Naval Postgraduate School
Monterey, CA 93940
(desires no CNWDI Documents)
Olcy Attn Code 0142 Library

Commanding Officer
Naval Research Laboratory
Washington, DC 20375
(RD & RD/N Attn Code 1221 for
& FRD Attn Code 2628 for)
Olcy Attn Code 2627 (Tech Lib)
Olcy Attn Code Boris/Book

Commander
Naval Sea Systems Command
Washington, DC 20362
Olcy Attn Sea-09G53 (Lib)
Olcy Attn Sea-0351

Officer In Charge
Naval Surface Weapons Center
White Oak Laboratory
Silver Spring, MD 20910
Olcy Attn Code F31
Olcy Attn H. Giaz

Commander
Naval Surface Weapons Center
Dahlgren, VA 22448
Olcy Attn Tech Library &
Infor Services Brnch

President
Naval War College
Newport, RI 02840
Olcy Attn Code E-11
(Tech Service)

Commander
Naval Weapons Center
China Lake, CA 93555
Olcy Attn Code 266 C Austin
Olcy Attn Code 3201 P Cordle
Olcy Attn Code 233 (Tech Lib)

Commanding Officer
Naval Weapons Evaluation Facility
Kirtland Air Force Base
Albuquerque, NM 87117
Olcy Attn R Hughes
Olcy Attn Code 10 (Tech Lib)

Office of Naval Research
Arlington, VA 22217
Olcy Attn Code 474 N Perron
Olcy Attn Code 715 (Tech Lib)
(Uncl only)

Office of the Chief of Naval
Operations
Washington, DC 20350
Olcy Attn OP 981
Olcy Attn OP 03EG

Director
Strategic Systems Project Office
Department of the Navy
Washington, DC 20376
Olcy Attn NSP-43 (Tech Lib)
Olcy Attn NSP-272

Air Force Geophysics Laboratory
Hanscom AFB, MA 01731
Olcy Attn LWW K Thompson

Air Force Institute of Technology
Air University
Wright-Patterson AFB, OH 45433
(Does not desire classified documents)
Olcy Attn Library

Headquarters
Air Force Systems Command
Andrews AFB
Washington, DC 20334
Olcy Attn DLW

Air Force Weapons Laboratory, AFSC
Kirtland AFB, NM 87117
Olcy Attn NTES-C R Henny
Olcy Attn NTED R Matalucci
Olcy Attn NTE M Plamondon
Olcy Attn R Guice
Olcy Attn SUL W Lee
Olcy Attn DEX

Assistant Chief of Staff
Intelligence
Department of the Air Force
Washington, DC 20330
Olcy Attn IN

Ballistic Missle Office/DE
Air Force Systems Command
Norton AFB, CA 92409
(Civil Engineering)
Olcy Attn DEB

Ballistic Missle Office/MN
Air Force Systems Command
Norton AFB, CA 92409
(Minuteman) MNNX
Olcy Attn MNNXH D Gage

Deputy Chief of Staff
Research, Development, & ACC
Department of the Air Force
Washington, DC 20330
Olcy Attn AFRDQSM

Deputy Chief of Staff
Logistics & Engineering
Department of the Air Force
Washington, DC 20330
Olcy Attn LEEE

Commander
Foreign Technology Division, AFSC
Wright-Patterson AFB, OH 45433
Olcy Attn NIIS Library

Commander
Rome Air Development Center, AFSC
Griffiss AFB, NY 13441
(Desires no CNWDI)
Olcy Attn TSLD

Stragetic Air Command/XPFS
Department of the Air Force
Offutt AFB, NB 68113
Olcy Attn NRI-STINFO Library
Olcy Attn XPFS

Department of Energy
Albuquerque Operations Office
P O Box 5400
Albuquerque, NM 87115
Olcy Attn CTID

Department of Energy
Washington, DC 20545
Olcy Attn OMA/RD&T

Department of Energy
Nevada Operations Office
P O Box 14100
Las Vegas, NV 89114
Olcy Attn Mail & Records for Technical Library

Department of the Interior
Bureau of Mines
Bldg. 20, Denver Federal Ctr
Denver, CO 80225
Olcy Attn Tech Lib (Uncl only)

Director
Federal Emergency Management Agency
1721 I Street, NW
Washington, DC 20472
Olcy Attn Hazard Eval & Vul Red Div

Aerospace Corp.
P O Box 92957
Los Angeles, CA 90009
Olcy Attn H Mirels
Olcy Attn Technical Infor Services

Agbabian Associates
250 N Nash Street
El Segundo, CA 90245
Olcy Attn M Agbabian

Analytic Services, Inc.
400 Army-Navy Drive
Arlington, VA 22202
Olcy Attn G Hesselbacher

Applied Theory, Inc.
1010 Westwood Blvd.
Los Angeles, CA 90024
(2cys if unclass or
lcy if class)
Olcy Attn J Trulio

Artec Associates, Inc.
26046 Eden Landing Road
Hayward, CA 94545
Olcy Attn S Gill

Avco Research & Systems Group
201 Lowell Street
Wilmington, MA 01887
Olcy Attn Library A830

BDM Corp.
7915 Jones Branch Drive
McLean, VA 22102
Olcy Attn A Lavagnino
Olcy Attn T Neighbors
Olcy Attn Corporate Library

BDM Corp.
P O Box 9274
Albuquerque, NM 87119
Olcy Attn R Hensley

Boeing Co.
P O Box 3707
Seattle, WA 98124
Olcy Attn M/S 42/37 R Carlson
Olcy Attn Aerospace Library

California Research & Technology, Inc.
6269 Variel Avenue
Woodland Hills, CA 91364
Olcy Attn Library
Olcy Attn K Kreyenhagen

California Research & Tech, Inc.
4049 First Street
Livermore, CA 94550
Olcy Attn D Orphal

Calspan Corp.
P O Box 400
Buffalo, NY 14225
Olcy Attn Library

Denver, University of
Colorado Seminary
Denver Research Institute
P O Box 10127
Denver, CO 80210
(Only lcy of class rpts)
Olcu Attn Sec Officer for
J Wisotski

EG&G Washington Analytical
Services Center, Inc.
P O Box 10218
Albuquerque, NM 87114
Olcy Attn Library

Eric H. Wang
Civil Engineering Rsch Fac
University of New Mexico
University Station
P O Box 25
Albuquerque, NM 87131
Olcy Attn N Baum

Gard, Inc.
7449 N Natchez Avenue
Niles, IL 60648
Olcy Attn G Neidhardt
(Uncl only)

General Electric, Co
Space Division
Valley Forge Space Center
P O Box 8555
Philadelphia, PA 19101
Olcy Attn M Bortner

General Electric Co.-Tempo
816 State Street (P O Drawer QQ)
Santa Barbara, CA 93102
Olcy Attn DASIAC

General Research Corp.
Santa Barbara Division
P O Box 6770
Santa Barbara, CA 93111
Olcy Attn B Alexander

Higgins, Auld Association
2601 Wyoming Blvd NE
Albuquerque, NM 87112
Olcy Attn J Bratton

IIT Research Institute
10 W 35th Street
Chicago, IL 60616
    Olcy Attn Documents Library
    Olcy Attn R Welch
    Olcy Attn M Johnson

Information Science, Inc.
123 W Padre Street
Santa Barbara, CA 93105
    Olcy Attn W Dudziak

Institute for Defense Analyses
400 Army-Navy Drive
Arlington, VA 22202
    Olcy Attn Classified Library

J H Wiggins Co., Inc.
1650 S Pacific Coast Highway
Redondo Beach, CA 90277
    Olcy Attn J Collins

Kaman Avidyne
83 Second Street
Northwest Industrial Park
Burlington, MA 01803
    Olcy Attn Library
    Olcy Attn E Criscione
    Olcy Attn N Hobbs
    Olcy Attn R Ruetenik

Kaman Sciences Corp.
P O Box 7463
Colorado Springs, CO 80933
    Olcy Attn F Shelton
    Olcy Attn Library

Kaman Sciences Corp.
Southern California Operations
101 Continental Blvd Suite 855
El Segundo, CA 90245
    Olcy Attn D Sachs

Lawrence Livermore National Lab.
P O Box 808
Livermore, CA 94550
    Olcy Attn DOC CON for L-200 T Butkovich
    Olcy Attn DOC CON for Tech Infor Dept. Library
    Olcy Attn DOC CON for L-205 J Hearst (Class L-203)
    Olcy Attn DOC CON for L-90 D Norris (Class L-504)
    Olcy Attn DOC CON for L-437 R Schock
    Olcy Attn DOC CON for L-7 J Kahn
    Olcy Attn DOC CON for L-96 L Woodruff (Class L-94)
    Olcy Attn DOC CON fro L-90 R Dong

Lockheed Missiles & Space Co., Inc.
P O Box 504
Sunnyvale, CA 94086
    Olcy Attn TIC-Library

Los Alamos National Scientific Lab.
Mail Station 5000
P O Box 1663
Los Alamos, NM 87545
    Olcy Attn MS 670/J Hopkins
    Olcy Attn DOC CON for M Sanpford
    Olcy Attn DOC CON for R Whittaker
    Olcy Attn DOC CON for MS 364
        (Class Reports Lib)
    Olcy Attn DOC CON for G Spillman
    Olcy Attn DOC CON for A Davis
    Olcy Attn DOC CON for R Bridwell

Lovelace Biomedical & Environmental
  Research Institute, Inc.
P O Box 5890
Albuquerque, NM 87115
    Olcy Attn R Jones (Unclas only)

Martin Marietta Corp.
P O Box 5837
Orlando, FL 32855
    Olcy Attn G Fotieo

McDonnell Douglas Corp.
5301 Bolsa Avenue
Huntington Beach, CA 92647
    Olcy Attn R Halprin

Merritt Cases, Inc.
P O Box 1206
Redlands, CA 92373
    Olcy Attn J Merritt
    Olcy Attn Library

Meteorology Research, Inc.
464 W Woodbury Road
Altadena, CA 91001
Olcy Attn W Green

Nathan M. Newmark Consult
Eng Services
B106A Civil Eng Bldg.
University of Illinois
Urbana, IL 61801
Olcy Attn N Newmark

Oak Ridge National Lab.
Nuclear Division
Z-10 Lab Records Div
P O Box X
Oak Ridge, TN 37830
Olcy Attn Civil Def Res Proj
Olcy Attn DOC CON for Central
Research Library

Pacifica Technology
P O Box 148
Del Mar, CA 92014
Olcy Attn G Kent
Olcy Attn R Bjork

Physics International Co.
2700 Merced Street
San Leandro, CA 94577
Olcy Attn E Moore
Olcy Attn L Behrmann
Olcy Attn Technical Library
Olcy Attn F Sauer

R & D Associates
P O Box 9695
Marina Del Rey, CA 90291
Olcy Attn Technical Infor Ctr
Olcy Attn A Latter
Olcy Attn A Kuhl
Olcy Attn J Carpenter
Olcy Attn C MacDonald
Olcy Attn R Port
Olcy Attn J Lewis

Rand Corp.
1700 Main Street
Santa Monica, CA 90406
Olcy ATTN C Mow

Sandia Laboratories
Livermore Laboratory
P O Box 969
Livermore, CA 94550
Olcy Attn DOC CON for Library
& Security Class Division

Sandia National Laboratories
P O Box 5800
Albuquerque, NM 87185
(Attn Mail Services Section
for Intended Recipient)
Olcy Attn Mail Ser Sec W Roherty
Olcy Attn Mail Ser Sec 3141
Olcy Attn Mail Ser Sec L Vortman
Olcy Attn Mail Ser Sec A Chaban
Olcy Attn Mail Ser Sec L Hill

Science Applications, Inc.
P O Box 2351
La Jolla, CA 92038
Olcy Attn Technical Library

Science Applications, Inc.
1257 Tasman Drive
Sunnyvale, CA 94086
Olcy Attn J Dishon

Science Applications, Inc.
2450 Washington Avenue
San Leabdro, CA 94577
Olcy Attn D Maxwell
Olcy Attn D Bernatein

Science Applications, Inc.
P O Box 1303
McLean, VA 22102
Olcy Attn M Knasel
Olcy Attn B Chambers III
Olcy Attn R Sievers
Olcy Attn J Cockayne

Southwest Research Institute
P O Drawer 28510
San Antonio, TX 78284
Olcy Attn W Baker
Olcy Attn A Wenzel

SRI International
333 Ravenswood Avenue
Menlo Park, CA 94025
Olcy Attn G Abrahamson

Systems, Science & Software, Inc.
P O Box 1620
La Jolla, CA 92038
Olcy Attn Library
Olcy Attn D Grine
Olcy Attn T Riney
Olcy Attn K Pyatt

Teledyne Brown Engineering
Cummings Research Park
Huntsville, AL 35807
    01cy Attn J Ravenscraft

Terra Tek, Inc.
420 Wakara Way
Salt Lake City, UT 84108
    01cy Attn Library
    01cy Attn S Green
    01cy Attn A Jones

Tetra Tech, Inc.
630 N Rosemead Blvd.
Pasadena, CA 91107
    01cy Attn L Hwang
    01cy Attn Library

TRW Defense & Space Sys Group
One Space Park
Redondo Beach, CA 90278
    01cy Attn I Alber
    01cy Attn Tech Infor Ctr
    02cy Attn N Lipner
    01cy Attn P Bhutta
    01cy Attn D Baer
    01cy Attn R Plebuch

TRW Defense & Space Sys Group
P O Box 1310
San Bernardino, CA 92402
    01cy Attn E Wong
    01cy Attn P Dai

Universal Analytics, Inc.
7740 W Manchester Blvd
Playa Del Rey, CA 90291
    01cy Attn E Field

Weidlinger Assoc., Consulting Eng
110 E 59th Street
New York, NY 10022
    01cy Attn M Baron

Weidlinger Assoc., Consulting Eng
3000 Sand Hill Road
Menlo Park, CA 94025
    01cy Attn J Isenberg

Westinghouse Electric Corp.
Marine Division
Hendy Avenue
Sunnyvale, CA 94088
    01cy Attn W Volz